

1
2
3
4
5
6
7
8
9
10
11
12
13
14
15
16
17
18
19
20
21
22
23

Benthic macrofaunal carbon fluxes and environmental drivers of spatial variability in a large coastal-plain estuary

Authors: Seyi Ajayi^{1*}, Raymond Najjar¹, Emily Rivest², Ryan Woodland³, Marjorie A.M. Friedrichs², Pierre St-Laurent², Spencer Davis¹

¹The Pennsylvania State University, University Park, PA, USA
²Virginia Institute of Marine Science, William & Mary, Gloucester Point, VA, USA
³University of Maryland Center for Environmental Sciences, Cambridge, MD, USA

Correspondence to: Seyi Ajayi (oa5061@psu.edu)

Abstract

While the importance of carbon cycling in estuaries is increasingly recognized, the role of benthic macrofauna remains poorly quantified due to limited spatial and temporal resolution in biomass measurements. Here, we ask: (1) To what extent do benthic macrofauna contribute to estuarine carbon cycling via respiration and calcification? and (2) How well can routinely collected environmental variables predict their biomass? We analyzed [data from](#) 8,128 benthic samples collected from the Chesapeake Bay between 1995 and 2022 and estimated associated carbon fluxes using empirical relationships. We then used generalized additive models to relate observed and modeled environmental variables to the biomass. Biomass was highest in the upper main stem of the Bay (Upper Bay) and upper Potomac River Estuary, the largest tidal tributary of the Bay. In the Upper Bay, benthic macrofauna respired 18–45% of the estimated organic carbon supply. Calcification-driven alkalinity reduction reached $6.31 \pm 2.84 \text{ mol m}^{-2} \text{ yr}^{-1}$ in the Potomac River Estuary, aligning with prior estimates of alkalinity sinks in the tributary and highlighting the potential importance of calcifying fauna in alkalinity dynamics. Estimated CO_2 production in the Upper Bay from benthic respiration and calcification ($151 \text{ g C m}^{-2} \text{ yr}^{-1}$) also exceeded observed air–sea CO_2 fluxes ($74.5 \text{ g C m}^{-2} \text{ yr}^{-1}$). Generalized additive models revealed that low salinity, moderate dissolved oxygen, and elevated nitrate best predicted high-biomass zones, with the three predictors explaining 52% of biomass deviance. These predictive relationships offer a pathway to estimate macrofaunal biomass and associated carbon fluxes in systems where direct biomass measurements are sparse. Our findings demonstrate that benthic macrofauna play a substantial and spatially structured role in estuarine carbon cycling. Incorporating their contributions into estuarine biogeochemical models will improve predictions of ecosystem responses to environmental and anthropogenic change.

1. Introduction

Benthic macrofauna are vitally important to estuarine ecosystems by improving water quality, producing and consuming organic matter, recycling nutrients, cycling pollutants, stabilizing and transporting sediment, and providing food for both human populations and estuarine organisms (Schratzberger & Ingels, 2018; Snelgrove, 1997; Wilson & Fleeger, 2023). Benthic macrofauna also play a role in estuarine carbon cycling through secondary production, respiration, and calcification. Secondary production refers to the consumption of organic matter by benthos to produce soft tissue biomass (Diaz & Schaffner, 1990; Dolbeth et al., 2012; Sturdivant et al., 2013). This biomass contributes to trophic transfer, as benthic organisms are consumed by predators or decomposers, with much of the associated organic carbon eventually being removed from the estuary through advection to the open ocean or burial in sediment (Diaz & Schaffner, 1990; Wilson & Fleeger, 2023). Respiration and calcification influence carbon cycling through their impact on the carbonate system, the chemical equilibrium governing the partitioning of inorganic carbon among its primary forms.

Impacts of respiration and calcification on the carbonate system are best understood via their impacts on two master variables, dissolved inorganic carbon (DIC) and total alkalinity (TA). DIC is a measure of the total concentration of inorganic carbon species in water, including CO₂, bicarbonate ion, and carbonate ion:

$$[DIC] = [CO_2] + [HCO_3^-] + [CO_3^{2-}]. \quad (1)$$

TA is the excess of proton acceptors over donors and reflects the capacity of a water body to buffer pH changes. For understanding impacts of biogeochemical processes, the form of TA known as the explicit conservative alkalinity (Glud, 2008; Wolf-Gladrow et al., 2007) is useful:

$$[TA] = [Na^+] + 2[Mg^{2+}] + 2[Ca^{2+}] + [K^+] + 2[Sr^{2+}] + \dots - [Cl^-] - [Br^-] - [NO_3^-] - \dots$$

Deleted: other

Deleted: often have limited mobility and, in some cases, long life spans, making them reliable indicators of local environmental variability caused by natural and anthropogenic stresses. Their relative abundance and diversity are often used as a proxy to describe the condition of estuaries (Dauer, 1993; Pearson & Rosenberg, 1978; Rosenberg, 1995; Weisberg et al., 1997).
→ In addition to shaping ecosystem structure and serving as indicators of environmental health, benthic macrofauna

Deleted: central

Deleted: . Through secondary

Formatted: Font color: Auto

Formatted: Font color: Auto

Formatted: Font color: Auto

Formatted: Font color: Auto

Deleted: , they influence carbon transport and the partitioning of carbon between organic and inorganic

Deleted: which describes

Deleted: and strongly regulates key biogeochemical variables, such as pH, calcium carbonate saturation state, and the partial pressure of carbon dioxide (pCO_2)....

88 $- \text{TPO}_4 + \text{TNH}_3 - 2\text{TSO}_4 - \text{THF} - \text{THNO}_2,$
 89 (2)

90 where the last five terms represent the total forms of phosphate, ammonia, sulfate, fluoride, and
 91 nitrite, respectively.

92 Respiration, unlike secondary production, directly alters the carbonate system.

93 Respiration is the metabolic process by which organisms break down organic matter to release

94 energy. ~~Aerobic respiration, produces carbon dioxide (CO₂), water, and energy with oxygen~~

95 ~~serving~~ as the terminal electron acceptor;

96 $\text{CH}_2\text{O} + \text{O}_2 \rightarrow \text{CO}_2 + \text{H}_2\text{O}.$ (3)

97 When oxygen becomes depleted, anaerobic respiration takes over, relying on alternative electron
 98 acceptors such as nitrate, sulfate, or iron oxides. For benthic macrofauna, oxygen is essential for
 99 respiration; anaerobic respiration in sediments is primarily mediated by microbes (Glud, 2008).

100 The CO₂ generated during aerobic respiration increases DIC (Equation 1). ~~Although aerobic~~

101 respiration ~~slightly decreases TA due to the regeneration of nitrate during organic matter~~

102 ~~remineralization, the effect is small (≈16 moles of NO₃⁻ per 106 moles of CO₂; Redfield, 1963).~~

103 During calcification, benthic organisms, such as bivalves, take up calcium (Ca²⁺) and

104 HCO₃⁻ to form calcium carbonate (CaCO₃) shells, releasing CO₂ and water as byproducts:

105 $\text{Ca}^{2+} + 2\text{HCO}_3^- \rightarrow \text{CaCO}_3 + \text{CO}_2 + \text{H}_2\text{O}.$ (4)

106 Although calcification increases CO₂ in the water column, it results in a net decrease in DIC,

107 since two moles of HCO₃⁻ are removed for every mole of CaCO₃ precipitated, while only one

108 mole of CO₂ is returned to the water column (Equation 1). The removal of Ca²⁺ also decreases

109 TA by twice the amount of DIC (Equation 2). Calcification is thermodynamically favored when

110 the calcium carbonate saturation state (Ω) exceeds 1.

111 $\Omega = \frac{[\text{Ca}^{2+}][\text{CO}_3^{2-}]}{K_{\text{sp}}}$

Deleted: In aerobic

Deleted: serves

Deleted: , producing carbon dioxide (CO₂), water, and energy...

Deleted: Though not shown in Equation 3,

Formatted: Font color: Auto

Deleted: also ultimately releases about

Deleted: nitrate (NO₃⁻) for every

Deleted: CO₂ produced (

Deleted: , which decreases TA (Equation 2). Anaerobic respiration, such as denitrification and sulphate reduction, which consume nitrate and TSO₄, respectively, increase TA (Equation 2)...

Formatted: Font color: Auto

Formatted: Font color: Auto

Deleted: The saturation state is defined as: $\Omega = \frac{[\text{Ca}^{2+}][\text{CO}_3^{2-}]}{K_{\text{sp}}}$

When $\Omega < 1$ (undersaturation), dissolution is favored, leading to the release of Ca^{2+} and CO_3^{2-} back into solution and increasing TA. Low Ω impairs shell formation and increases mortality in juveniles, regardless of pH or $p\text{CO}_2$ (Green et al., 2009; Thomsen et al., 2015; Waldbusser et al., 2015).

Building on these conceptual and mechanistic insights, field and modeling studies have revealed the potentially large influence of benthic macrofauna on estuarine carbon cycling, particularly through respiration and calcification. A compilation of data from 20 estuaries estimated that benthos (encompassing microbes, meiofauna, and macrofauna) respire approximately 24% of the total input of organic carbon, defined here as the sum of inputs of autochthonous (from primary production) and allochthonous (e.g., from rivers) organic carbon, (Hopkinson & Smith, 2004). An excess of benthic respiration over primary production observed in many estuaries implies significant allochthonous inputs (Hopkinson & Smith, 2004; Kemp et al., 1997; Schwinghamer et al., 1986). Benthic macrofauna, particularly bivalves, substantially contribute to benthic respiration and have been hypothesized to significantly decrease the phytoplankton and suspended particulate concentrations in estuaries (Cercio & Noel, 2010; Galimany et al., 2020; Nakamura & Kerciku, 2000; Newell & Ott, 2011).

In contrast to respiration, the impact of benthic calcification on estuarine carbon cycling remains underexplored (Waldbusser et al., 2013). However, large alkalinity sinks in estuarine tributaries suggest that calcifying organisms, such as bivalves, may play a substantial role (Najjar et al., 2020). The combined CO_2 production from respiration and calcification may also constitute a significant carbon flux to the atmosphere. In San Francisco Bay, this production is estimated to occur at twice the rate of CO_2 uptake by primary production, while global extrapolations indicate that these emissions may rival those from the world's lakes or planetary

Deleted: where

Deleted: is the solubility product, which varies with the form of calcium carbonate (typically aragonite or calcite), temperature, pressure, and salinity. ...

Deleted: Saturation state is the primary driver of calcification in bivalves, especially during early life stages when physiological control over acid-base balance is limited. ...

Deleted: 2, making bivalve recruitment particularly vulnerable in coastal systems prone to acidification...

Deleted: In addition to altering carbon chemistry through metabolic processes, benthic macrofauna also influence carbon cycling through physical mechanisms such as bioturbation, which is the physical reworking of sediments via burrowing, feeding, and irrigation. In the short term, such activity creates a heterogeneous sediment-water interface, characterized by tracks, fecal mounds, burrows, and funnels (Meysman et al., 2006). Over longer timescales, bioturbation acts as an effective mixing mechanism that homogenizes the upper sediment layers. This reworking alters redox gradients, enhances organic matter decomposition, and facilitates solute exchange between porewaters and the overlying water column (Glud, 2008). As a result, bioturbation can increase rates of respiration, promote the release of DIC, and influence carbonate chemistry by exposing calcareous material to undersaturated conditions, thereby enhancing dissolution (Middelburg, 2018). These physical processes play a critical but often underappreciated role in regulating sediment-water carbon dynamics.

Deleted: Respiration has been studied more extensively than calcification. ...

Deleted: This definition of the total input of organic carbon is used throughout the remainder of this paper. In a study of coastal seagrass meadows, macrofauna were found to account for 40% of total benthic respiration (Rodil et al. [1]

Deleted: Bivalves, in particular

Deleted: (

Deleted: Cercio & Noel (2010) modeled the effect of bivalve filter feeders in the Chesapeake Bay and found [2]

Deleted: recent discoveries of

Formatted: Font color: Auto

Deleted: be

Deleted: CO_2 consumption

Deleted: (Chauvaud et al., 2003). A

Formatted: Font color: Auto

Formatted: Font color: Auto

Formatted: Font color: Auto

Deleted: extrapolation of the CO_2 generated from calcifying benthos in estuaries is comparable to the magnitude of [3]

Formatted: Font color: Auto

Formatted: Font color: Auto

210 volcanism (Chauvaud et al., 2003). As previously described, although both respiration and
211 calcification generate CO₂, they have opposite effects on DIC: respiration increases DIC,
212 whereas calcification reduces it. Thus whether calcifying benthos act as a net source or sink of
213 DIC depends on the relative magnitudes of these two processes.

214 To quantify the magnitude of these benthic contributions to carbon cycling, researchers
215 often estimate rates of secondary production, respiration, and calcification based on benthic
216 biomass. Because secondary production can be time-consuming and costly to measure, it is often
217 estimated using empirical relationships that relate it to benthic biomass, incorporating variables
218 such as taxon, average body mass, and water temperature (Brey, 1990; Chauvaud et al., 2003;
219 Dolbeth et al., 2012; Edgar, 1990; Schwinghamer et al., 1986; Sturdivant et al., 2013; Tumbiolo
220 & Downing, 1994). Calcification and respiration rates can be inferred from these secondary
221 production estimates using empirical relationships or proportional scaling (Chauvaud et al.,
222 2003; Schwinghamer et al., 1986).

223 Despite their importance to carbon cycling, benthic macrofauna biomass is ~~rarely~~
224 measured ~~due to high cost and logistical challenges~~ (Pearson & Rosenberg, 1978; Snelgrove et
225 al., 2018). In contrast, environmental variables that influence benthic communities are typically
226 ~~measured~~ more frequently. To better incorporate benthic macrofaunal processes into carbon
227 budgets and numerical models, it is useful to assess how well these more readily available
228 environmental variables can serve as predictors of biomass.

229 There are many environmental influences on the distribution of benthic macrofauna.
230 Hypoxia (dissolved oxygen concentrations ≤ 2 mg L⁻¹) is a major stressor that reduces biomass,
231 alters community structure, and impairs key functions such as metabolism, bioturbation, and
232 calcification (Borja et al., 2008; Diaz et al., 1995; Diaz & Rosenberg, 2008; Levin et al., 2009;

Deleted: often sparsely

Deleted: across space and time

Deleted: the

Deleted: of benthic sampling

Deleted: collected

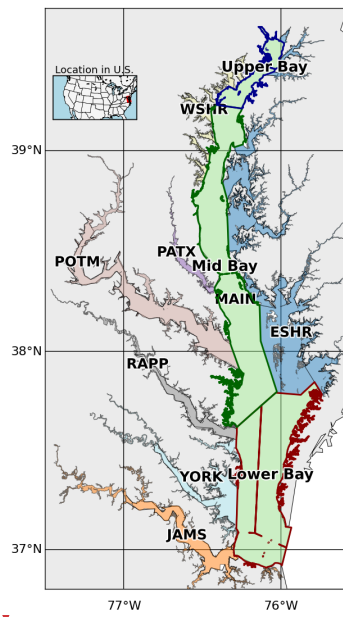
Deleted: and with greater spatial and temporal resolution

239 Murphy et al., 2011; Rousi et al., 2019; Seitz et al., 2009; Woodland & Testa, 2020). Benthic
240 macrofauna are particularly vulnerable due to their proximity to the sediment–water interface,
241 immobility, and limited capacity to avoid low-oxygen zones (Dauer & Alden, 1995; Vaquer-
242 Sunyer & Duarte, 2008). Behavioral and physiological responses to hypoxia differ among taxa,
243 with some groups like bivalves showing greater tolerance to short-term events (Seitz et al., 2009;
244 Vaquer-Sunyer & Duarte, 2008; Woodland & Testa, 2020). Salinity also plays a central role in
245 structuring benthic communities, with species distributions reflecting distinct physiological
246 tolerances (Dauer, 1993; Holland et al., 1987; Little et al., 2017; Seitz et al., 2009; Sturdivant et
247 al., 2013). Ocean acidification has been shown to negatively impact calcifying taxa, particularly
248 mollusks, by reducing growth, survival, and development (Birchenough et al., 2015; Jakubowska
249 & Normant-Saremba, 2015; Jansson et al., 2013; Kroeker et al., 2013; Thomsen et al., 2015).
250 Sediment characteristics also influence benthic biomass and diversity. Finer grain sizes and
251 higher organic content tend to be associated with lower biomass and biodiversity, whereas sandy
252 sediments are generally more favorable (Dauer & Alden, 1995; Grebmeier et al., 2015; Seitz et
253 al., 2009; Woodland & Testa, 2020). Finally, food availability, primarily from phytoplankton
254 production, strongly governs benthic biomass (Ehrnsten et al., 2019; Hagy, 2002; Kemp et al.,
255 2005; Pearson & Rosenberg, 1978). However, the relationship is complex, as high primary
256 production can also lead to oxygen depletion that ultimately suppresses benthic communities
257 (Dauer et al., 2000; Kemp et al., 2005). In summary, dissolved oxygen, salinity, ~~carbonate~~
258 chemistry, sediment composition, and food availability all serve as important environmental
259 predictors of benthic macrofauna biomass in estuarine ecosystems.

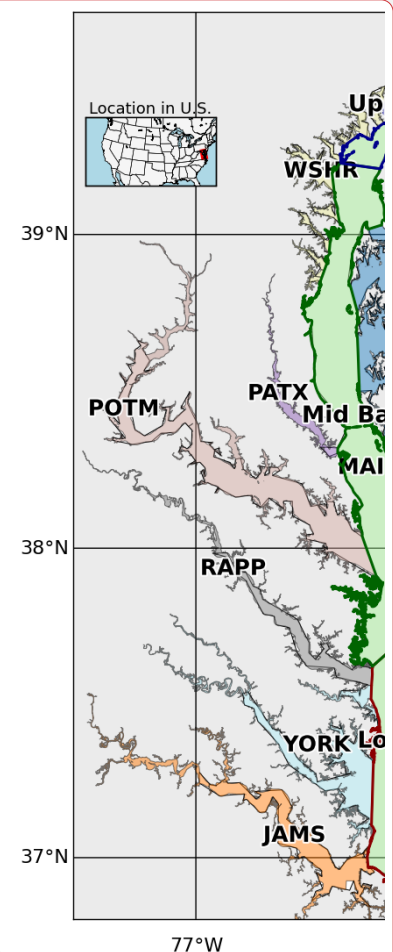
260 While numerous studies have examined the environmental drivers of benthic biomass in
261 estuaries, most have focused on relatively small spatial or temporal scales. Biomass, as opposed

Deleted: pH

263 to other metrics such as diversity and abundance, is particularly important because it is most
 264 directly related to estuarine carbon cycling processes (Cerco & Noel, 2010; Snelgrove, 1999).
 265 While benthic respiration has been widely quantified, estimates of benthic calcification remain
 266 rare (e.g., Chauvaud et al., 2003; Waldbusser et al., 2013), limiting our understanding of benthic
 267 contributions to carbon and alkalinity dynamics. The Chesapeake Bay, a large, coastal-plain
 268 estuary in the eastern United States (Fig. 1), provides a valuable case study due to its extensive
 269 historical monitoring data and diversity of carbon and alkalinity dynamics across its several tidal
 270 tributaries (Najjar et al., 2020). Although prior studies in the Bay have linked environmental
 271 variables to benthic biomass (Seitz et al., 2009; Woodland et al., 2021), these studies either used
 272 older datasets or focused on biomass primarily as a food source for higher trophic levels.



273
 274 Figure 1: Segmentation of the mainstem of the Chesapeake Bay and its tidal tributaries. The
 275 mainstem is divided into three regions, Upper Bay, Mid Bay, and Lower Bay. Acronyms denote



Deleted:
 Deleted: , based on geographic and ecological distinctions.

specific tributaries and sub-estuarine areas: ESHR refers to Eastern Shore tributaries, WSHR to Western Shore tributaries, POTM to the Potomac River, PATX to the Patuxent River, RAPP to the Rappahannock River, YORK to the York River system (including the Mattaponi and Pamunkey Rivers), and JAMS to the James River.

In our study, we build on this previous work by addressing the following research questions in the context of the Chesapeake Bay:

- 1) To what extent do benthic macrofauna contribute to estuarine carbon cycling through respiration and calcification, and how might these contributions vary across space?
- 2) How well can environmental variables routinely collected in estuarine monitoring programs predict benthic macrofauna biomass?

Answering these questions will help clarify the role of benthic macrofauna in estuarine carbon cycling and improve the ability of monitoring programs and numerical models to account for benthic processes using more accessible environmental data.

2. Methods

2.1 Overview

We examined historic benthic macrofauna biomass data collected annually by the Chesapeake Bay Long-Term Benthic Monitoring Program (BMP) (Dauer et al., 2000; Llansó & Zaveta, 2017). We applied empirical relationships linking biomass to secondary production, respiration, and calcification to quantify the impact of benthic macrofauna on carbon cycling in the Bay. To identify environmental predictors of benthic biomass, we compiled measurements of bottom water temperature, salinity, dissolved oxygen, and sediment sand fraction measured by the BMP at the same time and location as the benthic biomass samples. In addition to these measured environmental variables, we utilized output from ROMS-ECB, which is a three-

dimensional estuarine carbon and biogeochemistry (ECB) model embedded into the Regional Ocean Modeling System (ROMS; Shchepetkin & McWilliams, 2005) developed for the Chesapeake Bay (St-Laurent & Friedrichs, 2024b). We identified correlations between these environmental variables (observed and modeled) and benthic macrofauna biomass using generalized additive models (GAMs).

2.2 *Benthic biomass data*

Details of the BMP data we used in our study are described elsewhere (Dauer, 1993; Dauer et al., 2000; Dauer & Lane, 2010; Llansó & Scott, 2011; Llansó & Zaveta, 2017) and are summarized here. The program began in 1984, but consistency in sampling started in 1995. The sampling occurs mainly in the summer, between July 15 and September 30, at both fixed and random stations, with the latter changing location every year. The sampling is conducted separately by the states of Maryland (Llansó & Zaveta, 2017) and Virginia (Dauer & Lane, 2010), with slightly different protocols used in each state (see below). Our analysis spanned 1995 to 2022, the recent extent of available data, incorporating 28 years of data.

The Maryland monitoring program comprises 27 fixed and 150 random stations in the upper Chesapeake Bay. The Virginia monitoring program comprises 21 fixed and 100 random stations in the lower Chesapeake Bay. In Virginia, random stations were not sampled in 1995, and fixed stations were not sampled in 2017 or 2018. Water depths greater than 12 m in the mainstem part of the Bay in Maryland are not sampled because the bottom waters become anoxic in the summer, resulting in azoic sediments. The tributaries are sampled only in the tidal zone; areas with less than 1 m mean lower low water are considered non-tidal. Some locations, such as oyster reefs and other hard substrates, are also not sampled due to gear unsuitability in such habitats. To avoid seasonal biases, we excluded samples collected outside of the summer

325 sampling window of July 15–September 30, which occurred earlier in the study period. This
326 selection resulted in a dataset of 8128 samples across both states, or an average of 290 samples
327 per year, slightly less than the maximum of 298.

328 At each sampling station, the uppermost layers of sediment are collected. In Maryland,
329 the sites introduced in 1995 (two fixed sites and all random sites) are sampled with a Young
330 grab, which collects a surface area of 0.0440 m² to a depth of 0.10 m. For the other fixed sites in
331 Maryland, nearshore shallow sandy habitats of the mainstem and tributaries are sampled with a
332 modified box corer with a surface area of 0.0250 m² to a depth of 0.25 m. Muddy habitats and
333 deep-water habitats in the mainstem and tributaries of Maryland are sampled with a Wilco box
334 corer with a surface area of 0.0225 m² to a depth of 0.23 m. The fixed site in the Nanticoke River
335 is sampled with a Petite Ponar grab with a surface area of 0.0250 m² to a depth of 0.07 m. In
336 Virginia, fixed sites use a spade-type box-coring device with a surface area of 0.0182 m² to a
337 depth of 0.02 m; random sites use a Young grab with a surface area of 0.0400 m² to a depth of
338 0.10 m. One limitation of using multiple types of sampling gear is that differences in design,
339 such as penetration depth, sample volume, and sediment disturbance, can introduce variability in
340 estimates of benthic diversity, abundance, and biomass (Eleftheriou & Moore, 2013).

341 For both monitoring programs, the sampling contents are sieved through a 0.5 mm screen
342 to retain only benthic macrofauna. The macrofauna are identified at the lowest taxonomical
343 level. The specimens are dried on a pan for at least 24 hours to a constant weight, then a final
344 weight is measured. The specimens are then placed in a muffle furnace for 4 hours at 500 °C for
345 ashing, and the specimens are weighed again. The ash-free dry weight (AFDW), representing
346 only the soft-tissue biomass, is the difference between the dry and ashed weight. We converted
347 the AFDW in g per sample to biomass density *B* in units of g m⁻² by dividing the AFDW by the

area of the sampling device. The data used in our subsequent statistical analysis include the biomass density of individually selected species and classes and the total biomass density.

Benthic biomass is known to be highly patchy, with large variability even between samples taken in close proximity, hence the common use of replicate sampling in field protocols. To mitigate this noise and extract meaningful large-scale spatial patterns, we averaged across the 28-year time frame. All 8128 biomass samples collected from 1995 to 2022 were averaged onto a uniform grid with cells each measuring 0.04° in longitude and 0.03125° in latitude (~ 3.5 km per side). 1295 cells had at least one biomass measurement during the 28-year period. Across these cells, the average number of samples was 6.19, the median was 3, and the maximum was 69. Tributaries and the upper Bay were sampled more densely than the mainstem (Appendix A and Fig. A1). This “time-averaging” approach enabled clearer interpretation of spatial gradients in biomass and strengthened the robustness of subsequent statistical analyses aimed at identifying consistent environmental drivers. Some benthic biomass sampling stations fell outside the Chesapeake Bay Program (CBP) water quality segmentation scheme, which was originally developed to support monitoring and management analyses (Chesapeake Bay Program Analytical Segmentation Scheme: Revisions, Decisions and Rationales, 1983–2003, 2004). The CBP segments are defined at a relatively coarse spatial scale and often exclude narrow nearshore environments and small tributary creeks. To maintain consistency with the spatial framework used in coupled hydrodynamic–biogeochemical models, in our case ROMS-ECB, we excluded these points from analysis. This filtering step ensured that all biomass observations were aligned with the modeled domain, avoiding mismatches at the land–water interface. After this step, 1008 grid cells remained, of which 868 contained at least one biomass observation and the remainder were empty cells.

2.3 Carbon flux estimations

To estimate the impact of benthic macrofauna on carbon cycling, we applied empirical equations from the literature to quantify secondary production, calcification, and respiration. These equations were identified through an informal literature review using online tools (e.g., Google Scholar), with emphasis on studies relevant to soft-sediment bivalves, the dominant macrofauna in the Chesapeake Bay. We prioritized relationships applicable to local taxa and easily scalable to our biomass dataset. While multiple sources were available for secondary production, equations for respiration and calcification were more limited; in those cases, we selected models based on representative species that could be scaled from production estimates. We used a range of published values for biomass-to-carbon conversion, secondary production, and species-specific respiration and calcification ratios to estimate upper and lower bounds of carbon fluxes. Additional details on uncertainty calculations are provided in the Appendix B.

2.3.1 Secondary production

We converted biomass to secondary production \bar{S} (units of $\text{g C m}^{-2} \text{ yr}^{-1}$). Multiple approaches have been used for this conversion, and we used the average of three approaches to be able to broadly quantify uncertainty in our estimates.

In the first approach, secondary production is given by:

$$\bar{S}_1 = \alpha \bar{B}_c \quad (5)$$

where α is the specific growth rate and \bar{B}_c is carbon-based biomass (units of g C m^{-2}). We found three studies that estimated α for benthic macrofauna. At the low end, a study of benthic macrofauna in the Chesapeake Bay used $\alpha = 1.06 \text{ yr}^{-1}$ (Wilson & Fleeger, 2023). At the high end, a study of *C. fluminea* used $\alpha = 4.45 \text{ yr}^{-1}$ (Chauvaud et al., 2003). An intermediate value of $\alpha = 2 \text{ yr}^{-1}$ was based on monthly observations of benthic macrofauna dominated by the

394 crustacean *Corophium volutator* and the bivalve *Limecola balthica* at an intertidal site in the
 395 upper Bay of Fundy (Schwinghamer et al., 1986). A mean value of 2.50 yr⁻¹ was used in

396 Equation 5. $\overline{B_c}$ is computed from biomass \overline{B} (units of g m⁻²) using:

$$397 \quad \overline{B_c} = r_c \overline{B} \quad (6)$$

398 where r_c is the ratio of carbon mass to total mass in benthic organic matter. In a study on the
 399 bivalve filter feeders *Rangia cuneata* and *Corbicula fluminea*, which dominate in the tidal fresh
 400 and oligohaline waters of the Chesapeake Bay, $r_c = 0.47$ g C g⁻¹ was used (Cerco & Noel,
 401 2010). A slightly lower value of 0.41 g C g⁻¹ was used in a study of native and introduced
 402 bivalves in six North American freshwater systems (Chauvaud et al., 2003). A mean value of r_c
 403 = 0.44 g C g⁻¹ was used in our calculation.

404 In the second approach, temperature (T) dependence for bivalve secondary production
 405 was added (Sturdivant et al., 2013):

$$406 \quad S_2 = S_0 \left(\frac{B}{1 \text{ g m}^{-2}} \right)^{0.87} \left(\frac{T}{1 \text{ }^\circ\text{C}} \right)^{0.46} \quad (7)$$

407 where $S_0 = 0.40$ g C m⁻² yr⁻¹. Note that the coefficient at the beginning of the equation differs
 408 from that of Sturdivant et al. (2013) because of a change in units of \overline{B} from mg to g m⁻² and of \overline{S}
 409 from mg C d⁻¹ to g C m⁻² yr⁻¹. This equation has been shown to agree well with secondary
 410 production and biomass measurements (Sturdivant et al., 2013).

411 Finally, in the third approach (Tumbiolo & Downing, 1994), depth (Z) dependence was
 412 added:

$$413 \quad \begin{aligned} & \log_{10} \left(\frac{S_3}{1 \text{ g C m}^{-2} \text{ yr}^{-1}} \right) \\ &= \beta_0 + b \log_{10} \left(\frac{B}{1 \text{ g m}^{-2}} \right) - m \log_{10} \left(\frac{M}{1 \text{ mg}} \right) + t \left(\frac{T}{1 \text{ }^\circ\text{C}} \right) \\ & \quad - z \log_{10} \left(\frac{Z}{1 \text{ m}} + 1 \right) \end{aligned} \quad (8)$$

Deleted: 6

415 where $\beta_0 = 0.24, b = 0.96, m = 0.21, t = 0.03, z = 0.16$, and M is the maximum individual
416 body mass. Equation 8 was developed by Tumbiolo & Downing (1994) through multiple
417 regression analysis of 125 benthic invertebrate populations, including data from the Chesapeake
418 Bay. In their model, M refers to the maximum individual mass of the largest size class observed
419 within a population. It was identified as the second most important predictor of secondary
420 production after total biomass. Their analysis showed that species with greater maximum sizes
421 tend to have slower turnover rates and lower production-to-biomass ratios. In our application, we
422 treated M as a constant, based on the maximum individual mass of the bivalve *R. cuneata*
423 collected in a study in the Choptank River in the Chesapeake Bay, which was 5953 mg (Hartwell
424 et al., 1991). *R. cuneata* is among the most abundant and largest benthic macrofaunal species in
425 our study area (Cercio & Noel, 2010; Hartwell et al., 1991).

426 In Equations 7 and 8, we used the bottom water temperature measured on the same day
427 the benthic samples were collected. This reliance on summer temperature values represents a key
428 limitation of our study, as it likely leads to overestimation of annual secondary production,
429 particularly for Equation 8. For example, Equations 7 and 8 both predict maximum summer
430 secondary production that is about 5 times larger than the minimum winter production, assuming
431 an annual temperature range of 1 °C to 25 °C. However, we note that the first approach for
432 secondary production (Equation 6) has no temperature dependence. Figures C1–C3 in Appendix
433 C provide a detailed comparison of secondary production across the three models and assess
434 temperature effects on Models 2 and 3.

435 2.3.2 Calcification

436 Benthic macrofaunal calcification C (g $\text{CaCO}_3 \text{ m}^{-2} \text{ yr}^{-1}$) was computed from secondary
437 production following Chauvaud et al. (2003):

Deleted: 9

Deleted: 8

Deleted: 9

Deleted: 8

Deleted: 9

$$C = r_s S \quad (9)$$

where r_s is the ratio of shell CaCO_3 mass production to tissue organic C mass production, which has units of $\text{g CaCO}_3 (\text{g C})^{-1}$. Based on samples of the bivalve *Potamocorbula amurensis* in the northern San Francisco Bay, Chauvaud et al. (2003) found r_s to be $10 \text{ g CaCO}_3 (\text{g C})^{-1}$. They also cited a ratio of $15 \text{ g CaCO}_3 (\text{g C})^{-1}$ for the bivalve *C. fluminea*, a more relevant species to our study, but the reference is from unpublished data. We used the average of the two values, $12.5 \text{ g CaCO}_3 (\text{g C})^{-1}$, which corresponds to a molar ratio of $1.5 \text{ mol CaCO}_3 (\text{mol C})^{-1}$.

2.3.3 Respiration

The ratio of respiration to secondary production, expressed as energy fluxes, was derived from an empirical relationship between benthic macrofauna biomass and respiration in the Bay-of-Fundy study referenced earlier (Schwinghamer et al., 1986):

$$\log_{10} \left(\frac{R}{1 \text{ kcal m}^{-2} \text{ yr}^{-1}} \right) = \alpha_0 + s \log_{10} \left(\frac{S}{1 \text{ kcal m}^{-2} \text{ yr}^{-1}} \right) \quad (10)$$

where $s = 0.993$ and $\alpha_0 = 0.367$. Since s is nearly 1, the relationship simplifies to:

$$R = 10^{\alpha_0} S = 2.33S \quad (11)$$

Deleted: 12

Assuming that the conversion between carbon and energy is the same for S and R , this equation can be directly applied to these processes expressed as carbon fluxes, consistent with our other carbon flux estimates. Further, combining the relationships of calcification and respiration with secondary production on a molar basis allows a best estimate of the molar ratio of respiration to calcification: $2.33/1.5 = 1.55$.

2.3.4 Impact on the carbonate system

From the estimated benthic macrofaunal calcification (C) and respiration (R), we calculated TA and DIC fluxes (units of $\text{mol m}^{-2} \text{ yr}^{-1}$):

$$F_{TA} = \frac{-2C}{M_{CaCO_3}} \quad (12)$$

$$F_{DIC} = \frac{R}{M_C} - \frac{C}{M_{CaCO_3}} \quad (13)$$

where M_{CaCO_3} and M_C are the molar masses of $CaCO_3$ and C, respectively, and the sign convention is positive from the benthic fauna to the water column. Both calcification and respiration will lead to increases in the concentration of aqueous CO_2 , and so there is a CO_2 flux from benthic fauna that can be decomposed into CO_2 fluxes resulting from these two processes:

$$F_{CO_2} = F_{CO_2}^{TA} + F_{CO_2}^{DIC} \quad (14)$$

It has been estimated, assuming air–sea CO_2 equilibrium, that every mole of $CaCO_3$ precipitated leads to the evasion of 0.6–1 mole of CO_2 to the atmosphere, depending on the temperature, salinity, atmospheric pCO_2 , and initial alkalinity (Chauvaud et al., 2003; Frankignoulle et al., 1998; Ware et al., 1992).

In light of strong departures from air–sea CO_2 equilibrium in estuaries, including the Chesapeake Bay (Herrmann et al., 2020), we instead estimate the production rate of CO_2 using buffer factors, ζ_{TA} and ζ_{DIC} , which are defined as the fractional change in $[CO_2]$ divided by the fractional change in $[TA]$ and $[DIC]$, respectively; e.g., $\zeta_{TA} = (\Delta[CO_2]/[CO_2])/(\Delta[TA]/[TA])$. This approach also allows us to estimate the CO_2 flux from respiration. We computed the buffer factors in three steps. First, we used output from ROMS-ECB (described in more detail later in the Methods Section 2.4) for the years 1995–2022 and calculated long-term averages of bottom $[TA]$, $[DIC]$, temperature, salinity, and pressure (estimated from water depth) at each model grid cell. These values were used as input to PyCO2SYS (Humphreys et al., 2022) to calculate the baseline $[CO_2]$. Second, we individually perturbed $[TA]$ and $[DIC]$ by 1% ($\Delta[TA]$ and $\Delta[DIC]$)

487 while holding all other variables constant and recalculated $[\text{CO}_2]$ to get $\Delta[\text{CO}_2]$. Third, we
 488 computed ζ_{TA} and ζ_{DIC} using the definition of the buffer factors.

489 To relate the fluxes to the buffer factors, we use the flux form of the buffer factors:

$$490 \quad \zeta_{\text{TA}} = \frac{F_{\text{CO}_2}^{\text{TA}}/[\text{CO}_2]}{F_{\text{TA}}/[\text{TA}]} \quad (15)$$

$$491 \quad \zeta_{\text{DIC}} = \frac{F_{\text{CO}_2}^{\text{DIC}}/[\text{CO}_2]}{F_{\text{DIC}}/[\text{DIC}]} \quad (16)$$

492 These flux forms take the definitions of the buffer factors and replace ratios of concentration
 493 changes (e.g., $\Delta[\text{CO}_2]/\Delta[\text{TA}]$) with ratios of fluxes (e.g., $F_{\text{CO}_2}/F_{\text{CO}_2}^{\text{TA}}$). Using Equations 15 and 16
 494 in Equation 14 yields an expression for the CO_2 flux from benthic fauna to the water column:

$$495 \quad F_{\text{CO}_2} = [\text{CO}_2] \left(\frac{\zeta_{\text{TA}} F_{\text{TA}}}{[\text{TA}]} + \frac{\zeta_{\text{DIC}} F_{\text{DIC}}}{[\text{DIC}]} \right). \quad (17)$$

496 2.3.5 Spatial analysis and comparison to other carbon fluxes

497 To place benthic macrofauna contributions to estuarine carbon cycling in a broader
 498 spatial context, we averaged fluxes over 10 regions based on aggregated Chesapeake Bay
 499 Program segments (Fig. 1): the major tidal tributaries (the Patuxent, Potomac, Rappahannock,
 500 York, and James River Estuaries), the Western and Eastern Shores, and the Upper, Mid, and
 501 Lower (mainstem) Bay. Additionally, we computed averages over the mainstem Bay and the
 502 whole Bay. For each region, we calculated benthic respiration and bivalve calcification rates
 503 based on observed biomass, using the empirically derived equations just described. We then
 504 compared these fluxes to other components of the estuarine carbon budget using published
 505 values for primary production, allochthonous organic carbon inputs, oyster calcification, and air–
 506 sea gas exchange.

Deleted: 16

Deleted: 17

Deleted: 15

510 First, we assessed the extent to which benthic macrofauna remineralize organic carbon
511 inputs by comparing our calculated respiration rates to net primary production (NPP) and
512 external particulate organic carbon (POC) loads. Primary production and POC values were
513 obtained from prior studies (Herrmann et al., 2015; Kemp et al., 1997; Najjar et al., 2018; Zhang
514 & Blomquist, 2018) and scaled to match the spatial extent of our biomass data. In the Upper Bay,
515 we calculated organic carbon inputs by distributing the Susquehanna River's POC load over the
516 combined surface area of the oligohaline and tidal fresh segments (CB1 and CB2, (Olson, 2012)).
517 This approach assumes that the majority of the annual POC load from the Susquehanna River
518 remains concentrated in the Upper Bay and is respired rather than transported downstream, an
519 assumption supported by Canuel & Hardison (2016). For comparison, we also distributed
520 Susquehanna River POC inputs across the entire mainstem. For brevity, we restricted our
521 tributary-level comparison to the Potomac River Estuary, where the full organic carbon load was
522 distributed across the surface area of the entire tidal tributary (Fig. 1).

523 Second, we compared our soft-sediment bivalve calcification estimates to published
524 oyster calcification rates from (Fulford et al., 2007). Oyster ash-free dry weight was converted to
525 live weight using a 10:1 ratio (Mo & Neilson, 1994), and a calcification rate of 2 mg CaCO_3 per
526 g live weight per day was applied (Waldbusser et al., 2013). Because Eastern oyster (*Crassostrea*
527 *virginica*) populations in the Chesapeake Bay were historically at least two orders of magnitude
528 higher than current levels (Fulford et al., 2007; Newell, 1988), we also scaled published oyster
529 calcification rates up by a factor of 100 to estimate potential historical contributions. This
530 comparison allowed us to place present-day bivalve calcification into the broader context of
531 ecosystem function.

532 Third, we evaluated whether riverine calcium supply could limit observed calcification
533 by estimating annual calcium fluxes from the Susquehanna and Potomac Rivers using non-tidal
534 USGS data from 1995 to 2022 and the Weighted Regression on Time, Discharge, and Season
535 (WRTDS) method (Hirsch et al., 2010). Assuming a 1:1 molar ratio between Ca^{2+} and CaCO_3
536 formation, we estimated the maximum potential calcification that could occur if all incoming
537 calcium were used for shell production in adjacent estuarine zones.

538 Finally, we compared CO_2 generated from respiration and calcification (Equation 17) to
539 published estimates of air–sea CO_2 exchange (Chen et al., 2013; Herrmann et al., 2020).

540 The estimated carbon fluxes reveal important spatial patterns, but their interpretation
541 should be tempered by uncertainty in several underlying assumptions. While secondary
542 production models are relatively well-calibrated across estuarine systems, the calculations for
543 calcification and respiration are more sparse and less empirically constrained. Our propagated
544 uncertainty in calcification and respiration incorporates variation in biomass-based carbon
545 content, multiple conversion approaches from biomass to secondary production, and calcification
546 parameters derived from two different bivalve species. Although we used different methods to
547 estimate calcification and propagated these uncertainties accordingly, only one approach was
548 available for respiration.

549 We estimated uncertainties in F_{DIC} and F_{TA} , which represent the propagated uncertainties
550 from respiration and calcification alone, with no additional sources of uncertainty included in
551 those calculations. However, we did not calculate formal uncertainties in F_{CO_2} due to the
552 complexity involved. Additional uncertainty in F_{CO_2} arises from the use of annually averaged,
553 model-derived values for salinity, temperature, depth, DIC, and TA. Further uncertainty stems

Deleted: 18

555 from the method used to calculate δ from TA and DIC perturbations. While these additional
556 sources contribute to the overall uncertainty in F_{CO_2} , the uncertainties in F_{DIC} and F_{TA} are likely
557 to remain the dominant contributors.

558 The resulting error bars in the various carbon fluxes reflect these methodological
559 uncertainties, offering a plausible range rather than precise values. Thus, the benthic macrofaunal
560 carbon fluxes presented here should be interpreted with some caution, with more confidence
561 given to the broad spatial patterns and less to the absolute values.

562 ***2.4 Environmental predictors of benthic biomass***

563 From the BMP, we used bottom temperature, salinity, and dissolved oxygen data, which
564 are measured with a YSI 660 Sonde or Hydrolab DataSonde 4a in Maryland and a YSI 85 Model
565 meter in Virginia 1 m above the sediment surface. Extreme outliers, defined as data points that
566 fall beyond three times the interquartile range from the first or third quartile, were removed. As a
567 result, one value for dissolved oxygen and one for water temperature were excluded from the
568 analysis. The salinity zones are also characterized at each site as tidal fresh (<0.5 ppt),
569 oligohaline (0.5–5 ppt), low mesohaline (5–12 ppt), high mesohaline (12–18 ppt), and polyhaline
570 (>18 ppt); these zones are relatively geographically fixed (with some changes in 2011 due to
571 Hurricane Irene and Tropical Storm Lee) based on long-term averages of salinity (Llansó, 2002;
572 Llansó & Zaveta, 2017). Sediment sand fraction was measured by first collecting two 120 ml
573 benthic grab sub-samples. Sand particles are separated by wet-sieving through a 63- μ m stainless
574 steel sieve. Sand fraction is recorded after drying and weighing the samples. The bottom water
575 quality and sediment composition data were time-averaged using the same scheme described
576 earlier for the benthic biomass data.


ROMS-ECB output was used to characterize environmental variables not measured by the BMP that could be relevant to predicting the benthic macrofauna biomass distribution. ROMS-ECB uses 20 terrain-following vertical levels and a uniform horizontal resolution of 600 m (St-Laurent & Friedrichs, 2024b). We compiled daily averaged output at various grid points from 1995 to 2022 corresponding to the locations of each of the 8128 benthic biomass samples. We selected the ROMS output at the nearest ROMS grid point to each BMP sample location for each variable of interest, described below. Several ROMS-ECB environmental variables are directly linked to primary production, but the timing of peak primary production does not always align with periods of greatest food availability for benthic organisms. To capture ecologically meaningful variation in benthic–pelagic coupling, we calculated both seasonal and annual averages for each variable. Seasonal groupings reflect key ecological periods: spring (March–May), which includes the diatom bloom that delivers fresh organic material to the benthos, and summer (June–August), characterized by stratification, hypoxia, and intense remineralization. Fall (September–November) and winter (December–February) were also included to represent background seasonal variability. We then time-averaged the seasonal and annual means as described earlier. Coverage dropped from 868 to 846 cells after adding ROMS-ECB outputs, largely where the model masks shallow/tributary cells or lacks complete seasonal data.

We used ROMS-ECB output, as opposed to data from the Chesapeake Bay Water Quality Monitoring Program (WQMP), which has measured water quality variables since 1984 at over 100 tidal stations (Chesapeake Bay Program, n.d.). However, the stations are at different locations than the BMP stations, requiring interpolation to correlate these data with benthic biomass. Other studies have opted to use kriging, a method used to spatially interpolate surface water quality data, to increase the spatial resolution. Kriging has been found to outperform the

standard inverse distance weighting tools typically used in the Chesapeake Bay (Murphy et al., 2015). One study evaluated the kriging of surface WQMP data for July 2007 using 117–123 data points (Murphy et al., 2015). In cross-validation, one measured sample is removed, and the interpolation is then performed at that location; the interpolated value is then compared to the observed value. Cross-validation of temperature, salinity, and dissolved oxygen yielded root-mean-square errors (RMSE) of 0.75 °C, 1.1 ppt, and 1.2 mg L⁻¹, respectively. In contrast, ROMS-ECB output was evaluated with over 500,000 WQMP data points at multiple depths and locations from 1985 to 2021 (St-Laurent & Friedrichs, 2024a). The RMSEs for temperature, salinity, and dissolved oxygen were 1 °C, 1.9 psu, and 1.5 mg L⁻¹, respectively. Although these RMSEs are slightly higher than those from kriging, the evaluation was much more robust, and the long time series evaluation is more relevant to our time-averaging technique over 28 years. In addition, we wanted to utilize bottom water quality data, as these variables are measured closer to the location of benthic macrofauna. However, cross-validation for kriging was only performed at the surface (Murphy et al., 2015), possibly due to the challenges of accounting for bottom topography in spatial interpolation.

ROMS-ECB simulates many variables, and we considered the subset that might be good predictors of benthic biomass: bottom POC, bottom total suspended solids (TSS), and surface NO₃⁻. POC was considered because a large fraction of POC represents food for benthic macrofauna. TSS was considered a metric of suspended inorganic material, which can inhibit filter-feeding organisms (Grant & Thorpe, 1991). Photosynthesis is largely limited by NO₃⁻ in the Chesapeake Bay (Zhang et al., 2021); because phytoplankton productivity and the subsequent sinking of POC is an important source of organic matter to the benthos, NO₃⁻ could be a predictor of benthic biomass. ROMS-ECB output was evaluated for robustness with WQMP data

623 using Spearman's rank correlation coefficient, R_s , which measures the strength of the association
624 between two variables (Hauke & Kossowski, 2011). In our analysis of benthic biomass
625 predictors, we included only variables with R_s above 0.7, which generally indicates a strong
626 association (Akoglu, 2018). NO_3^- was used as it had $R_s = 0.77$, whereas POC and TSS were not
627 as they had $R_s = 0.26$ and 0.24 , respectively (St-Laurent & Friedrichs, 2024a).

628 We also considered potentially good predictors that could be computed from ROMS-
629 ECB output: surface oxygen supersaturation (ΔO_2) and bottom aragonite saturation state (Ω_{arag}).
630 ΔO_2 can be used as a tracer for net ecosystem production (Herrmann et al., 2020) and hence may
631 indicate organic matter availability to the benthos. $\Delta[\text{O}_2]$ is equal to O_2 minus the saturation
632 concentration, which was computed from temperature and salinity (Garcia & Gordon, 1992).
633 Positive ΔO_2 values are favored during net autotrophy (photosynthesis exceeds respiration),
634 while negative values are favored during net heterotrophy (respiration exceeds photosynthesis);
635 temperature change and transport can also create non-zero ΔO_2 . Ω_{arag} could predict benthic
636 biomass because bivalve calcification is expected to depend on this metric (Thomsen et al.,
637 2015).  PyCO2SYS (Humphreys et al., 2022) was used to derive the solubility product and
638 carbonate ion concentration from alkalinity, DIC, temperature, salinity, and water depth. We
639 examined ΔO_2 and Ω_{arag} in the subsequent statistical analysis because the ROMS-ECB output
640 variables used to compute them all had $R_s > 0.7$. Although calcium measurements were not
641 available for model evaluation, it is highly correlated to salinity, though deviations may occur at
642 low salinity (Beckwith et al., 2019).

643 **2.5 Statistical modeling of benthic biomass**

644 We used GAMs to evaluate how bottom water quality and biogeochemical model outputs
645 predict the spatial distribution of benthic macrofaunal biomass. GAMs are data-driven statistical

Deleted: Ω_{arag} is given by Equation 5, with

Deleted: corresponding to aragonite.

models that have been widely applied in coastal ecology since the late 20th century (Guisan et al., 2002; Smith et al., 2023). They model additive, smoothed relationships between predictor and response variables, making them well-suited for capturing the non-linear, non-monotonic patterns often observed in ecological datasets (Grüss et al., 2014; Guisan et al., 2002; Hastie & Tibshirani, 1987; Wood, 2017). GAMs also quantify the strength and relative contribution of each predictor (Guisan et al., 2002) and have demonstrated predictive performance comparable to or exceeding other modeling approaches (Drexler & Ainsworth, 2013). We used the *mgcv* package in R and applied restricted maximum likelihood (REML) to optimize smoothness (Wood, 2011; Wood, 2017). This approach is particularly effective with large datasets like ours, enabling robust estimation of spatial patterns in biomass across a broad geographic region (Grüss et al., 2014; Wood, 2011). Although GAMs can handle non-normal distributions of the response variable (Guisan et al., 2002), we found the best model fit by applying a natural logarithmic transformation to the biomass. A small constant (0.0001 g m^{-2}) was added to the biomass values before applying the natural logarithmic transformation to account for zeros in the data.

As described earlier, we initially identified eight environmental variables: O_2 , salinity, total depth, water temperature, sand fraction, NO_3^- , Ω_{arag} , and $\Delta[\text{O}_2]$. To avoid multicollinearity, which can distort GAM results (Grüss et al., 2014; Grüss et al., 2018; Guisan et al., 2002), we used Pearson's correlation coefficients (r) to evaluate the linear correlation between the predictor variables. When two variables were highly correlated ($r > 0.7$) (Dormann et al., 2013), we retained the variable that was more directly measurable and broadly understood across estuarine systems. Based on this assessment, we excluded Ω_{arag} and $\Delta[\text{O}_2]$ due to their strong correlation with other variables and retained the remaining six variables for GAM analysis. While necessary for model stability, this approach may limit the explanatory power of the GAM by excluding

671 ecologically meaningful predictors. The full list of candidate variables and their inclusion status
672 is provided in Table 1.

673 Table 1: Predictor variables from the Chesapeake Bay Benthic Monitoring Program and ROMS-
674 ECB compiled from 1995–2002. For ROMS-ECB output, daily values were used to calculate
675 annual averages and seasonal averages for spring (March–April), summer (July–August), fall
676 (September–November), and winter (December–February)

Dataset	Location	Variable	Units	Processing	Used in GAMs?
BMP	Bottom	O ₂	mmol m ⁻³	Removed extreme outliers	Yes
BMP	Bottom	Salinity	ppt	None	Yes
BMP	Bottom	Total depth	m	None	Yes
BMP	Bottom	Water temperature	°C	Removed extreme outliers	Yes
BMP	Bottom	Sand fraction	%	None	Yes
ROMS-ECB	Surface	NO ₃ ⁻	mmol m ⁻³	Annually and seasonally averaged	Yes
ROMS-ECB	Bottom	POC	mmol m ⁻³	Annually and seasonally averaged	No, model evaluation gave poor results

ROMS- ECB	Bottom	TSS	mg L ⁻¹	Annually and seasonally averaged	No, model evaluation gave poor results
ROMS- ECB	Bottom	Ω_{arag}		Calculated from alkalinity, DIC, temperature, water depth, and salinity using PyCO2SYS. Annually and seasonally averaged	No, highly correlated with salinity
ROMS- ECB	Surface	$\Delta[\text{O}_2]$	mmol m ⁻³	Calculated from oxygen, salinity and temperature using Gracia & Gordon (1991, 1992). Annually and seasonally averaged	No, highly correlated with salinity and NO_3^-

677 We used Akaike's Information Criterion (AIC), a statistical measure that has been
678 increasingly used in ecology, to evaluate which combination of parameters results in the best
679 model fit (Symonds & Moussalli, 2011). AIC is calculated using the number of fitted parameters
680 in the model, the maximum likelihood estimate, and the residual sum of squares (Symonds &
681 Moussalli, 2011). Among the candidate models, the one with the lowest AIC value offers the
682 best balance between explanatory power and simplicity, requiring the fewest necessary

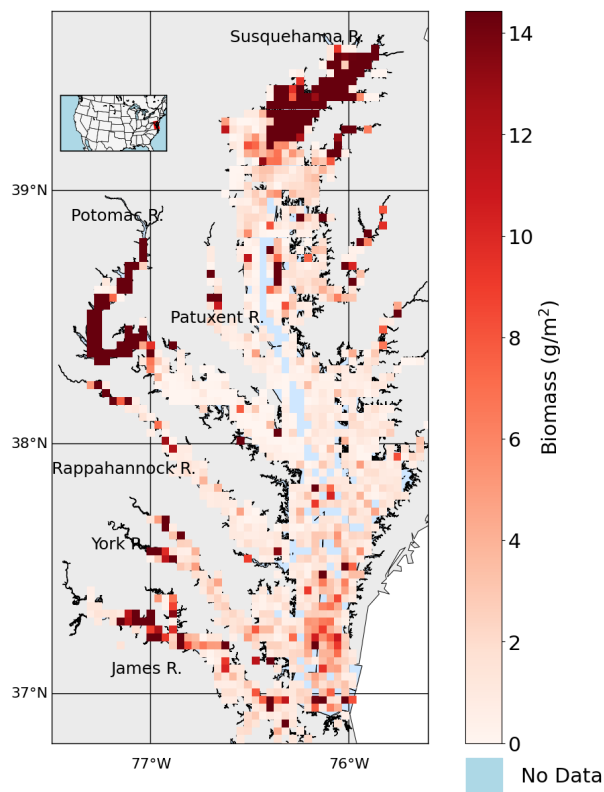
parameters. We chose the assemblage of predictor variables in our model that minimized AIC. We generally used annually averaged predictor variables from the ROMS-ECB output because using seasonal averages had a negligible difference on the AIC. To assess the relative influence of each predictor variable, we used Akaike weights, which indicate the probability that a given model is the best among those considered. We ranked models by AIC and summed the Akaike weights for all models containing each predictor variable. Higher Akaike weights indicate stronger support for a variable's inclusion in the best-fitting models. Interaction terms between predictor variables were examined, but their inclusion did not significantly improve the AIC values.

3. Results

3.1 *Spatial distribution of benthic macrofauna biomass*

The time-averaged (1995–2022) summer benthic macrofauna biomass exhibits strong spatial variability across the Chesapeake Bay, with higher concentrations in the tidal fresh and oligohaline zones, and lower concentrations in the Mid Bay and lower sections of many tributaries (Figure 2, 3a). The arithmetic mean of all biomass measurements based on the full data set, $N = 8128$ is 7.93 g m^{-2} (median = 0.98 g m^{-2}), whereas the spatial mean across all grid cells with at least one biomass measurement ($N = 1295$) is 7.16 g m^{-2} (median = 1.39 g m^{-2}). The sampling scheme oversamples the tidal tributaries (Fig. A1), where biomass density is higher, inflating the arithmetic mean. The standard deviation of the full dataset is 28.7 g m^{-2} , indicating that the distribution is heavily skewed to the right, with the highest sample reaching up to 722 g m^{-2} . The standard deviation of the time-averaged data is 18.0 g m^{-2} , considerably smaller than the full data set since it does not include temporal variability, but is nevertheless still skewed to the right, with the highest gridded value of 220 g m^{-2} . Most of the high-biomass density zones

706 ($>30 \text{ g m}^{-2}$) are concentrated in the tidal fresh and oligohaline sections of the mainstem and
707 Potomac River Estuary. The other tributaries have higher biomass in the tidal fresh and
708 oligohaline and zones compared to the other salinity zones. In the Mid Bay and lower sections of
709 many tributaries, biomass is very low.



710
711 Figure 2: Average summer biomass density from 1995 to 2022 from the Chesapeake Bay
712 Benthic Monitoring Program. Biomass values are shown using a red color scale, white represents
713 0 g m^{-2} , light blue indicates open water grid cells with no data, and gray represents land areas
714 with no data.

715 The distribution of the biomass into salinity zones for multiple taxonomic groups and
716 species is shown in Fig. 3b–f. Bivalves dominate biomass in all salinity zones, except the
717 polyhaline, where they are comparable to polychaetes. Bivalves comprise 88.0% of the benthic
718 biomass, and polychaetes comprise 7.3%. At a taxonomic species level, the bivalve *R. cuneata*
719 comprises 66.1% of the biomass, followed by the bivalves *C. fluminea* (8.0%) and *L. balthica*
720 (7.5%). Appendix D provides a more detailed spatial analysis of species distribution. The high-
721 biomass zones in the Upper Bay, Potomac River Estuary, and James River Estuary are
722 dominated by *R. cuneata*, mostly in the oligohaline zone (Figs. 3c & D1). *C. fluminea* also
723 dominates in relatively higher quantities in the tidal fresh zone of the Potomac River Estuary and
724 the tidal fresh zone of the Upper Bay (Figs. 3d & D1). In general, *R. cuneata* has a higher
725 biomass density in the tidal fresh than *C. fluminea* because *R. cuneata* is present in all tidal fresh
726 zones. *L. balthica* is distributed in multiple salinity zones; it is highest in the lower mesohaline
727 and is the dominant species in the lower mesohaline zone of the Upper Bay and Patuxent River
728 Estuary (Figs. 3e & D1). The biomass density of *L. balthica* in the lower mesohaline ($<2 \text{ g m}^{-2}$)
729 is significantly lower than that of *C. fluminea* and *R. cuneata* in the tidal fresh and oligohaline
730 zones. Polychaetes are the species that dominate over the largest geographic area, throughout the
731 polyhaline and part of the higher mesohaline (Figs. 2, 3f, & D1). However, their biomass density
732 is low relative to bivalves ($<2 \text{ g m}^{-2}$). Bivalves are sparse throughout the higher mesohaline and
733 polyhaline zones.

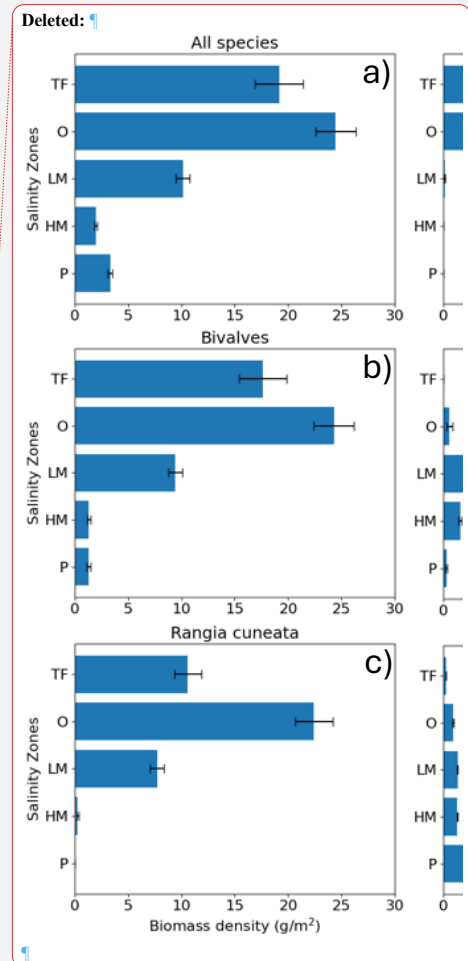
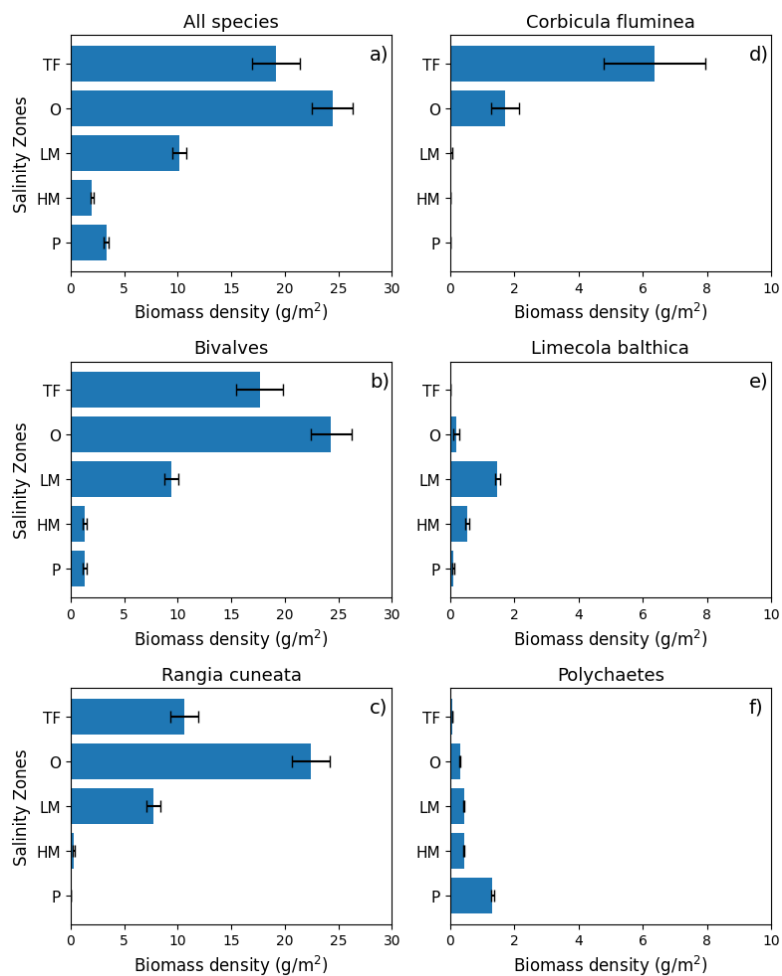


Figure 3: Average summer benthic biomass density of multiple classes and species in each salinity zone from 1995 to 2022. The salinity zones are determined by the BMP based on the long-term average of salinity in each geographic zone: TF – Tidal Freshwater (0–0.5 ppt), O – Oligohaline (0.5–5 ppt), LM – Low Mesohaline (5–12 ppt), HM – High Mesohaline (12–18 ppt), and P – Polyhaline (≥ 18 ppt). Averages and standard errors (bars) are computed using the full

743 data set, not the gridded values. Note the difference in horizontal scale between the left and right
744 columns.

745 3.2 Carbon flux estimates

746 Average benthic macrofaunal carbon and alkalinity fluxes vary across the 10 regions of
747 the Bay (Fig. 4). Among the different fluxes, which are all presented on a molar basis in Figure
748 4, $\overline{F_{TA}}$ has the largest magnitude, followed, in decreasing order, by $\overline{F_{CO_2}}$, respiration (R/M_C),
749 calcification (C/M_{CaCO_3}), and $\overline{F_{DIC}}$. We first discuss calcification, respiration, $\overline{F_{TA}}$, and $\overline{F_{DIC}}$.
750 Calcification is 1.55 times respiration (best estimate), as a result of the molar ratio of these
751 processes (Section 2.3.3). $\overline{F_{TA}}$ is always negative, as expected because calcification is an
752 alkalinity sink, and twice the magnitude of calcification (Equation 12). The best estimate of $\overline{F_{DIC}}$
753 was mostly positive, though it could be positive or negative because calcification is a DIC sink
754 and respiration is a DIC source (Equation 13). The best estimate of $\overline{F_{DIC}}$ ends up being positive
755 because respiration exceeds calcification. Using the best estimate of the molar
756 respiration:calcification ratio (1.55) and Equations 12 and 13, it can be shown that $-\overline{F_{TA}}/\overline{F_{DIC}} =$
757 3.6, consistent with the results in Fig. 4. Estimated uncertainties (Appendix B) were
758 approximately 45% for calcification, 40% for respiration, 135% for $\overline{F_{DIC}}$, and 45% for $\overline{F_{TA}}$. The
759 uncertainty for $\overline{F_{DIC}}$ being greater than 100% admits the possibility of negative DIC fluxes.
760 $\overline{F_{CO_2}}$ is always positive because benthic macrofauna remove TA from and add DIC to the
761 water column. The magnitude of $\overline{F_{CO_2}}$ can be understood by first noting that it is proportional to
762 $\overline{F_{TA}}$ and $\overline{F_{DIC}}$, with proportionality constants of $[\text{CO}_2]\zeta_{TA}/[\text{TA}]$ and $[\text{CO}_2]\zeta_{DIC}/[\text{DIC}]$,
763 respectively (Equation 17; note that $\overline{F_{TA}} < 0$ and $\zeta_{TA} < 0$, leading to $\overline{F_{CO_2}} > 0$). In the open ocean,
764 using mean conditions of $p\text{CO}_2 = 400 \mu\text{atm}$, $[\text{TA}] = 2300 \mu\text{mol kg}^{-1}$, temperature = 15 °C, and
765 salinity = 35, we can use carbonate system equilibria to estimate $[\text{CO}_2] \sim 15 \mu\text{mol kg}^{-1}$, $[\text{DIC}] \sim$

Deleted: 13

Deleted: 14

Deleted: 13

Deleted: 14

Deleted: 18

771 $2100 \mu\text{mol kg}^{-1}$, and $-\zeta_{\text{TA}} \sim \zeta_{\text{DIC}} = 11$, which leads to F_{CO_2} about 7–8% of $-F_{\text{TA}}$ and F_{DIC} . Here,
 772 we are seeing F_{CO_2} comparable in magnitude to F_{TA} and F_{DIC} because Bay waters tend to have
 773 higher $[\text{CO}_2]$ and ζ_{DIC} and lower $[\text{TA}]$ and $[\text{DIC}]$ than what is observed in open-ocean waters, as
 774 we show in Appendix E and Fig. E1. We observe much larger F_{CO_2} in tidal fresh (6–18 mol m^{-2}
 775 yr^{-1}) compared to oligohaline (3–7 $\text{mol m}^{-2} \text{yr}^{-1}$) waters (Fig. 4), despite comparable values of
 776 F_{DIC} and F_{TA} . These differences in F_{CO_2} between tidal zones are primarily driven by $[\text{CO}_2]$,
 777 which is much higher in the tidal fresh due to a lower TA:DIC ratio (Fig. E11). The magnitudes
 778 of the buffer factors are also greater in lower salinity waters (Figs. E1g & E1h), decreasing
 779 slightly in the polyhaline. Polyhaline values (13–16) are comparable to oceanic estimates of 9–15
 780 (Eggleston et al., 2010).

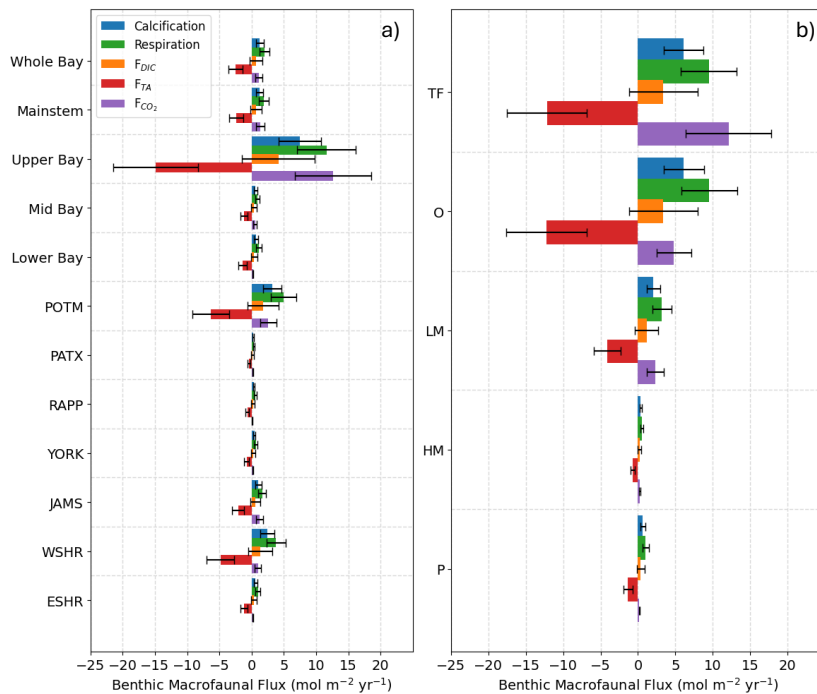


Figure 4: Average benthic macrofaunal fluxes by (a) Bay region and (b) salinity zone. Tributary and sub-estuarine acronyms: ESHR – Eastern Shore tributaries; WSHR – Western Shore tributaries; POTM – Potomac River; PATX – Patuxent River; RAPP – Rappahannock River; YORK – York River system (including Mattaponi and Pamunkey Rivers); JAMS – James River. Salinity zone abbreviations: TF – Tidal Freshwater (0–0.5 ppt), O – Oligohaline (0.5–5 ppt), LM – Low Mesohaline (5–12 ppt), HM – High Mesohaline (12–18 ppt), P – Polyhaline (≥ 18 ppt). Error bars represent uncertainty ranges (Appendix B).

In multiple segments of the Bay, benthic macrofaunal respiration rates (R) are comparable to the total available organic carbon supply, defined here as the sum of net primary production (NPP) and riverine POC loads (Table 2). In the Upper Bay, benthic macrofaunal respiration rates are within the range of NPP alone. When combined with POC loads, our estimates suggest that benthic macrofauna respire approximately $f = 18\text{--}45\%$ of the total available organic carbon, where:

$$f = \frac{R}{NPP + POC} \quad (18)$$

$$\frac{\Delta f}{f} = \sqrt{\left(\frac{\Delta R}{R}\right)^2 + \left(\frac{\Delta NPP}{NPP}\right)^2} \quad (19)$$

Here, ΔR and ΔNPP are the standard errors of R and NPP , respectively. This formulation is consistent with the uncertainty propagation approach described in Appendix B.

In the Potomac River Estuary, respiration rates exceed external organic carbon loads, although NPP estimates for this region were unavailable. By contrast, in the mainstem and across the Bay as a whole, benthic respiration rates are much smaller than NPP, accounting for only 3–

802 8% of the total inputs of organic carbon to the mainstem. These percentages were calculated
803 using the same approach as in Equations 18–19, but substituting mainstem benthic macrofaunal
804 respiration, NPP, and POC inputs.

Deleted: -20

805 Table 2: Riverine POC load, net primary production (NPP), and benthic respiration compiled
806 from the listed studies compared with benthic macrofaunal respiration from our study. POC load
807 estimates from Zhang & Blomquist (2018) were based on USGS river monitoring data combined
808 with flow-weighted sediment and organic carbon concentrations. For POC loads we specifically
809 used values from Table S5 of Zhang & Blomquist (2018), which reports long-term average true-
810 condition annual loads. Susquehanna loads were distributed across the mainstem and Upper Bay,
811 Potomac River loads were distributed across the Potomac, and total watershed load was
812 distributed across the whole Bay. These loads were divided by the surface area of the
813 corresponding segment area (Chesapeake Bay Program, 2004) NPP values from Harding et al.
814 (2002) were derived from depth-integrated in situ ¹⁴C-uptake incubations across multiple cruises,
815 scaled using statistical models. Benthic respiration values from Kemp et al. (1997) were
816 estimated by combining seasonal in situ measurements of sediment oxygen consumption with
817 sulfate reduction rates, together accounting for microbial and macrofaunal respiration.

Region	Carbon Flux	Value (g C m ⁻² yr ⁻¹)	Reference
Whole Bay	Riverine POC load	12.0	Zhang & Blomquist (2018)
	Benthic macrofaunal respiration	24 ± 9	This study
Mainstem	Riverine POC load	18.8	Zhang & Blomquist (2018)
	NPP	385 ± 17	Harding et al. (2002)
	Benthic respiration	163.1	Kemp et al. (1997)
	Benthic macrofaunal respiration	22 ± 9	This study
Upper Bay	Riverine POC load	257.7	Zhang & Blomquist (2018)
	NPP	182 ± 27	Harding et al. (2002)

	Benthic respiration	44.3	Kemp et al. (1997)
	Benthic macrofaunal respiration	139 ± 55	This study
Potomac	Riverine POC load	31.9	Zhang & Blomquist (2018)
	Benthic macrofaunal respiration	59 ± 24	This study

819 Benthic macrofauna also contribute substantially to the calcium budget of the Bay. We
820 estimate that calcification by benthic macrofauna monitored in the BMP is slightly lower than
821 historical (pre-decline) estimates of the Eastern oyster (*Crassostrea virginica*) calcification in the
822 mainstem Bay but exceeds post-decline estimates by about 7 to 19 times in the Upper Bay (Table
823 3). This range was calculated by taking the upper and lower bounds of our measured calcification
824 rates (mean ± uncertainty) and dividing each by the post-decline oyster calcification rate.
825 Evaluating the role of bivalve calcification in utilizing calcium further underscores its
826 biogeochemical significance. Relative to annual riverine calcium fluxes, benthic macrofauna
827 would use ~22–58% of the available calcium in the Upper Bay and nearly all in the Potomac
828 River. These percentages were likewise calculated by taking the lower and upper bounds of our
829 measured calcification rates (mean ± uncertainty) and dividing each by the corresponding
830 maximum potential riverine calcium input, which was treated as fixed.

831 Table 3: Historic oyster calcification rates and estimated maximum potential calcification based
832 on riverine calcium input, compared with calcification rates from this study. Riverine calcium
833 load from the Susquehanna River was distributed across the Upper Bay and across the mainstem,
834 calcium load from the Potomac River was distributed within the Potomac segment, and the sum
835 of all riverine calcium inputs was distributed across the Whole Bay.

Region	Calcification Rate	Value (g CaCO ₃ m ⁻² yr ⁻¹)	Reference
Whole Bay	Riverine Ca load	135	USGS
	Benthic macrofauna	142 ± 62	This study
Mainstem	Riverine Ca load	213	USGS

	Oysters	139	Fulford et al. (2007); Waldbusser et al. (2013)
	Benthic macrofauna	120 ± 54	This study
Upper Bay	Riverine Ca load	1861	USGS
	Oysters	57	Fulford et al. (2007); Waldbusser et al. (2013)
	Benthic macrofauna	747 ± 329	This study
Potomac	Riverine Ca load	262	USGS
	Benthic macrofauna	316 ± 142	This study

836 The role of benthic macrofaunal metabolic processes in the carbon budget is particularly
837 pronounced when the effects of calcification and respiration are combined to estimate CO₂
838 production. This CO₂ flux exceeds the amount of outgassing estimated in the Upper Bay and the
839 mainstem overall (Table 4).

840 Table 4: Air–sea gas exchange from the listed studies compared with total benthic macrofaunal
841 CO₂ flux calculated in our study.

Region	CO ₂ Flux	Value (g C m ⁻² yr ⁻¹)	Reference
Whole Bay	Benthic macrofauna	13 ± 10	This study
Mainstem	Air–sea exchange	14.5 (outgassing)	Herrmann et al. (2020)
	Benthic macrofauna	16 ± 13	This study
Upper Bay (CB1– CB3) ^a (CB1 & CB2) ^a	Air–sea exchange	74.5 (outgassing)	Herrmann et al. (2020)
	Benthic macrofauna	151 ± 121	This study

842 ^a CB1–CB3 refer to Chesapeake Bay Program segmentation units (Chesapeake Bay Program,
843 2004): CB1 = tidal fresh, CB2 = oligohaline; CB3 = mesohaline.

844 3.3 Correlation of environmental variables with biomass

845 The GAMs analysis, based on gridded, time-averaged biomass data, revealed key drivers
846 of benthic biomass both at the community level (all taxa combined) and for specific taxonomic
847 groups and species. The results for total benthic biomass (all taxa), polychaetes, and the bivalve
848 species *R. cuneata*, *C. fluminea*, and *L. balthica* are shown in Table 5. The bivalve group was

849 excluded from the table because its results were nearly identical to total benthic biomass results.

850 For total benthic biomass, the predictor variables (O_2 , salinity, total depth, water temperature,

851 sand fraction, and NO_3^-) explain 54.9% of the deviance in biomass. For individual taxa, the

852 predictive capability of GAMs increases, with 73.7% of *R. cuneata* biomass deviance explained

853 by the predictor variables. For total benthic biomass, dissolved oxygen emerged as the strongest

854 predictor (with the highest summed Akaike weight), followed by total depth, salinity, and NO_3^- .

855 Although water temperature and sand fraction were included in the model, they had relatively

856 little influence. For individual taxa, dissolved oxygen became less influential, especially for *R.*

857 *cuneata* and *C. fluminea*. Salinity generally increased in influence as a predictor variable for

858 species-specific models, most notably for *C. fluminea*. NO_3^- also generally increased in influence

859 as a predictor variable for species-specific models, with very high influence as a predictor of *C.*

860 *fluminea* biomass.

861 Table 5: The best-fitting generalized additive model (GAM) for each taxa assemblage,

862 determined by minimizing Akaike’s Information Criterion (AIC). $N = 846$ (number of grid boxes

863 with data) for all models. Summed Akaike weights indicate the relative importance of each

864 predictor variable across all models considered, with higher values suggesting stronger support

865 for a variable’s inclusion in the best-fitting models. “N/A” indicates that the variable was not

866 included in the best model. Some variables may have high summed Akaike weights even if they

867 are not in the best-fitting model. For example, in the *R. cuneata* model, O_2 has a summed Akaike

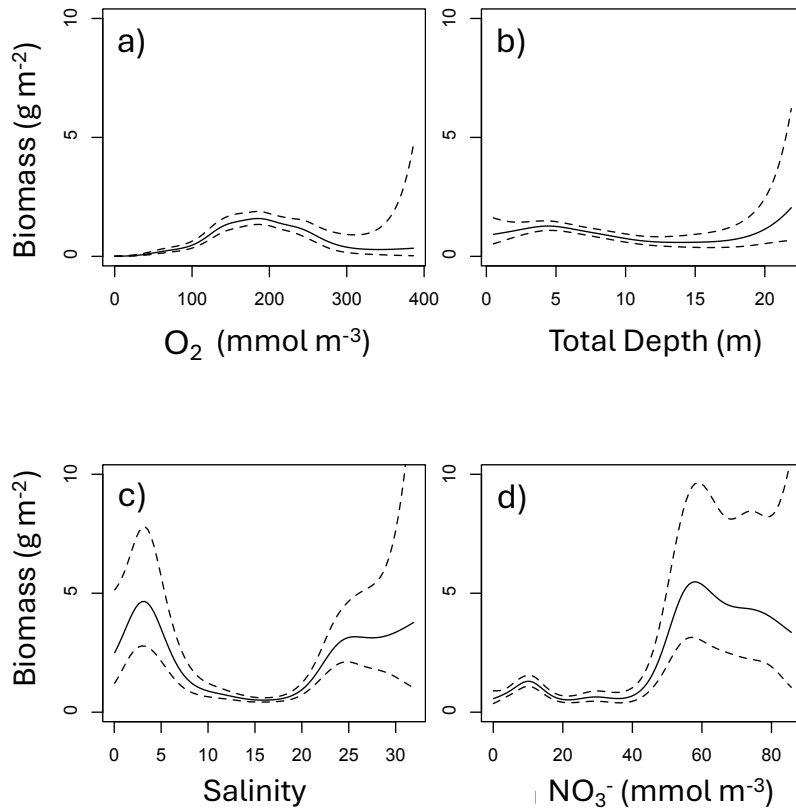
868 weight of 0.571, while water temperature has 0.032. In the *C. fluminea* model, O_2 has 0.384, and

869 total depth has 0.24.

Taxa	Deviance Explained	Summed Akaike Weight

		O ₂	Salinity	Total Depth	Water temperature	Sand fraction	NO ₃ ⁻
All taxa	54.9%	0.536	0.032	0.400	0.000	0.000	0.031
Polychaetes	50.0%	0.457	0.173	0.266	N/A	0.000	0.104
<i>R. cuneata</i>	73.7%	N/A	0.161	0.183	N/A	0.024	0.059
<i>C. fluminea</i>	65.9%	N/A	0.212	N/A	0.122	0.078	0.132
<i>L. balthica</i>	58.4%	0.888	0.000	0.112	N/A	0.000	0.000

870 The relative effects of O₂, salinity, NO₃⁻ and total depth on benthic biomass varied
871 considerably, as shown in the partial plots of Figure 5. Macrofauna biomass reaches its lowest
872 values at low dissolved oxygen, the only section of all the partial plots that reach 0 g m⁻².
873 Biomass is generally higher at shallower depths, although the effect is small. Biomass is highest
874 at both low and high salinities and high surface NO₃⁻. In summary, biomass is highest at
875 moderate dissolved oxygen, shallow depths, low or high salinities, and high NO₃⁻.



876
 877 Figure 5: Partial plots of the effect of significant predictor variables on total biomass: (a) bottom
 878 dissolved oxygen, (b) total depth, (c) bottom salinity, and (d) surface nitrate. Water temperature
 879 and sand fraction were included in the model but omitted from display as they did not
 880 significantly improve the model fit. The solid black line shows the response and the dashed lines
 881 show the 95% confidence interval. The natural log transformation was removed from biomass to
 882 enhance viewing of the partial plots. The x-axis was cut off at the upper quartile plus three
 883 interquartile ranges in order to remove extreme outliers from the plots.

884 The model fit evaluation, presented in Appendix F and Fig. F1, reveals some systemic
885 biases. The residuals (observed values minus model-fitted values) are slightly skewed to the left
886 (Fig. F1b), meaning the model is more likely to overestimate biomass. The response vs. fitted
887 value scatter plot shows a nearly linear relationship (Fig. F1a). The map of residuals (Fig. F1c)
888 shows that there is also an underestimation in the model fit at the high biomass zones, especially
889 in the Upper Bay.

890 **4. Discussion**

891 *4.1. Benthic macrofaunal contributions to the Chesapeake Bay carbon budget*

892 The higher benthic biomass in less saline waters of the Chesapeake Bay suggests a
893 significant role for respiration in the carbon budget in this region. The proportion of the total
894 input of particulate organic carbon that is respired by benthic macrofauna estimated in our study
895 in the Upper Bay (18–45%) is similar to the 14 to 40% range estimated for bivalve filter feeders
896 in tidal fresh and oligohaline waters by Cerco & Noel (2010). In the Upper Bay, where the
897 benthic macrofauna respiration is comparable to NPP, if all the NPP were respired solely by
898 benthic macrofauna, net ecosystem production would be zero. However, given the consideration
899 of additional respiration by other organisms (e.g., microbes and pelagic zooplankton) the
900 allochthonous POC from the Susquehanna River must be a critical source of organic carbon
901 driving net heterotrophy in this region. These findings reinforce the earlier conclusion that high
902 biomass zones in the Upper Bay are sustained by allochthonous organic inputs. The Potomac
903 River Estuary, however, presents a less conclusive case, partly due to the lack of available NPP
904 estimates. In this estuary, where benthic macrofaunal respiration exceeds the estimated POC
905 flux, additional carbon sources, such as autochthonous NPP or tidal wetland outwelling, may be
906 contributing to carbon metabolism. Notably, Herrmann et al. (2015) estimated that the amount of

907 organic carbon exported through wetland outwelling is approximately equal to half of that
908 exported by streamflow in Mid-Atlantic estuaries, highlighting its potential significance in
909 supporting heterotrophic processes in the Potomac.

910 Benthic macrofaunal respiration plays a smaller role in the rest of the Bay, where
911 autochthonous organic carbon dominates. For both the mainstem and the whole Bay, the
912 estimated primary production far exceeds the average estimated benthic macrofaunal respiration .
913 Kemp et al. (1997) estimated benthic respiration by combining sulfate reduction and sediment
914 oxygen consumption rates, which together account for both microbial and macrofaunal
915 respiration. Their results suggest that benthic respiration is a smaller fraction of NPP in the Mid
916 and Lower Bay, compared to the Upper Bay. This may reflect the relatively modest role of
917 macrofaunal respiration in these lower-biomass regions, despite higher autochthonous production
918 and organic carbon delivery to the sediments. Our estimates of benthic macrofaunal respiration
919 as a fraction of the total input of organic carbon to the mainstem (3–8%) is slightly lower than
920 estimates derived by Hopkinson & Smith (2004) and Rodil et al. (2022). Hopkinson & Smith,
921 (2004) estimated that approximately 24% of total available organic carbon is respired by the
922 benthos, while Rodil et al. (2022) found that benthic macrofauna account for roughly 40% of
923 total benthic respiration. Taken together, these studies suggest that around 10% of the total input
924 of organic carbon is expected to be respired by benthic macrofauna. Although the Bay-wide
925 fraction is small, macrofaunal respiration may still dominate locally in specific hotspots.

926 Unlike the extensive research on estuarine benthic respiration, benthic macrofaunal
927 calcification has received relatively little attention. Yet our findings suggest it may play a
928 significant role in the Chesapeake Bay carbon budget. As shown in Table 3, bivalves sampled
929 through the BMP program contribute substantially to calcification, surpassing calcification by

930 present-day Eastern oyster populations but comparable to that of historic populations in the
931 mainstem Bay. The importance of bivalve calcification is further emphasized when considering
932 calcium dynamics. To place bivalve calcification in context, we assumed that all riverine calcium
933 inputs were available for shell production. This is an upper-bound estimate because oceanic
934 calcium greatly exceeds riverine fluxes (Beckwith et al., 2019). While not a full calcium budget,
935 the comparison highlights how large the demand from calcification could be relative to the much
936 smaller riverine supply. Alkalinity fluxes further highlight the biogeochemical significance of
937 calcification. For the whole Bay, our estimated alkalinity consumption from benthic macrofaunal
938 calcification of $2.52 \pm 1.13 \text{ mol m}^{-2} \text{ yr}^{-1}$ ($6.90 \pm 3.10 \text{ mmol m}^{-2} \text{ day}^{-1}$) accounts for more than half
939 of the Bay-wide alkalinity sink estimated by Waldbusser et al. (2013) at $12 \text{ mmol m}^{-2} \text{ day}^{-1}$. In
940 the Potomac River Estuary, our estimated alkalinity sink due to benthic calcification
941 ($6.31 \pm 2.84 \text{ mol m}^{-2} \text{ yr}^{-1}$ or $17.29 \pm 7.78 \text{ mmol m}^{-2} \text{ day}^{-1}$) is comparable to the alkalinity sink of
942 $22 \pm 1 \text{ mmol m}^{-2} \text{ day}^{-1}$ estimated by Najjar et al. (2020), who proposed that *C. fluminea* was
943 primarily responsible. Our findings, highlighting contributions from both *R. cuneata* and *C.*
944 *fluminea*, support their hypothesis and emphasize the substantial role of benthic calcification in
945 modulating alkalinity in estuaries.

946 Benthic macrofauna may play a major role in CO₂ outgassing, as indicated by our
947 estimated CO₂ fluxes from benthic macrofauna in the Upper Bay and upper tributaries, which
948 exceed typical CO₂ fluxes at the air–sea interface. Our benthic macrofaunal CO₂ generation
949 estimates for the Upper Bay ($151 \text{ g C m}^{-2} \text{ yr}^{-1}$), where bivalve biomass is concentrated, exceed
950 those reported by Chauvaud et al. (2003), who estimated $55 \pm 51 \text{ g C m}^{-2} \text{ yr}^{-1}$ of CO₂ production
951 from calcification and respiration by the bivalve *P. amurensis* in northern San Francisco Bay.
952 Our results support their hypothesis that benthic calcifiers can serve as major CO₂ generators in

estuaries. Not all of this CO₂ generated would be outgassed. However, the combination of a TA sink and DIC source from the bivalves leads to elevated $p\text{CO}_2$, enhancing the potential for increased CO₂ outgassing (Middelburg et al., 2020). Given the high heterotrophy in the Upper Bay and upper tributaries, as well as the balance between benthic macrofaunal respiration and the total input of organic carbon to the Potomac River Estuary, it is conceivable that benthic macrofauna are major contributors to CO₂ outgassing in these regions.

Although our empirical framework presented here captures the dominant patterns of benthic secondary production, it does not explicitly incorporate seasonal temperature variability. Because we applied summer temperatures associated with biomass, our production estimates likely represent the upper end of expected values. A simple sensitivity analysis comparing summer and winter conditions suggests that production, and by extension calcification and respiration, may be closer to 60% of the values reported here under mean annual cycles. Importantly, this potential bias is encompassed within our uncertainty bounds and therefore does not affect our overall conclusions.

4.2. Environmental controls on benthic biomass distribution

Bivalve species distribution within the Bay is primarily driven by salinity tolerances. Both the GAMs analysis (Table 5) and the biomass densities associated with salinity zones (Fig. 3) showed that benthic biomass, dominated by bivalves, was much higher at lower salinities. The strong influence of salinity on benthic fauna distribution within estuaries has long been recognized (Cain, 1975; Hopkins et al., 1973). This relationship is illustrated in our study by the preference of the most abundant species, *R. Cuneata*, *L. balthica*, and *C. fluminea*, for less saline water. *R. Cuneata* is widely known to need less saline waters, optimally between 1 and 15 ppt, to survive (Hopkins et al., 1973). *C. fluminea* prefers freshwater environments (Phelps, 1994; Sousa

976 et al., 2008). *L. balthica* has a range of tolerances but abundance declines below 5 ppt (Jansson et
977 al., 2015). In our study, *L. balthica* is more concentrated between 5 and 13 ppt. While salinity
978 determines which species dominate, other factors influence their relative abundances within
979 salinity zones.

980 Within mesohaline zones, summer hypoxia appears to be driving extremely low benthic
981 biomass. In our GAMs analysis, an association existed between low biomass and extremely low
982 bottom dissolved oxygen values. Among the different salinity zones, low biomass is associated
983 with low dissolved oxygen in the high mesohaline, where we had the lowest biomass densities.
984 Long-term exposure to hypoxia ($<2 \text{ mg L}^{-1}$ or 62.5 mmol m^{-3}) is often fatal to benthic
985 macrofauna (Diaz et al., 1995; Seitz et al., 2006; Seitz et al., 2009) and many benthic
986 communities (approximately 50%) only recover on an annual timescale (Diaz et al., 1995). In
987 other words, regions that suffer frequent hypoxia often see lower levels of benthic biomass even
988 when hypoxic conditions are not occurring. In the Chesapeake Bay, hypoxia is most likely to
989 occur in the deeper, mesohaline regions (Frankel et al., 2022; Zheng & DiGiacomo, 2020),
990 providing evidence that our suppressed values of benthic macrofauna at this salinity zone could
991 be due to mass mortality from hypoxia. This pattern is particularly evident where biomass is
992 extremely low through the Mid Bay and lower Potomac River Estuary, regions typically
993 associated with summer hypoxia (Sturdivant et al., 2013).

994 Across the Bay, the relatively narrow range of summer bottom water temperatures likely
995 explains why temperature has an insignificant effect on the spatial distribution of benthic
996 biomass. In our GAMs analysis, summer bottom water temperature was not significantly
997 correlated with benthic biomass. Water temperature has been considered an important driver of
998 benthic biomass (Marsh & Tenore, 1990; Seitz et al., 2006; Seitz et al., 2009; Testa et al., 2020),

999 with low temperature specifically creating mass mortality of *R. cuneata* during winter and spring
1000 (Tuszer-Kunc et al., 2020). Higher temperature, however, will drive early and larger seasonal
1001 hypoxia in the Chesapeake Bay (Hinson et al., 2022; Irby et al., 2018; Ni et al., 2019). So,
1002 temperature could still indirectly affect benthic biomass through its effect on dissolved oxygen.
1003 Therefore, while temperature may not directly drive spatial patterns of biomass, it could be
1004 more relevant to temporal changes in biomass.

1005 Although NO_3^- is a strong predictor of benthic biomass, the mechanisms are likely
1006 complex and not necessarily linked to autochthonous primary production. In upper estuarine
1007 zones, high NO_3^- concentrations are often associated with elevated suspended solid loads, which
1008 limit light and may inhibit autotrophy (Brush et al., 2020b). Yet these same areas show strong
1009 heterotrophy, suggesting that respiration exceeds local production. Prior studies have shown that
1010 POC in upper estuaries contains substantial terrigenous inputs (Canuel & Hardison, 2016), and
1011 respiration of this organic matter likely contributes to heterotrophy in these regions (Kemp et al.,
1012 1997; Testa et al., 2020). This pattern raises the possibility that NO_3^- may serve as a proxy for
1013 allochthonous POC delivery. Supporting this, USGS data compiled by Zhang & Blomquist
1014 (2018) indicate that tributaries with high NO_3^- also tend have high loads of POC. However,
1015 further study is needed to test this hypothesis, and the observed NO_3^- –POC correlation should
1016 not be interpreted as causal.

1017 Our model explained roughly half of the deviance in biomass, indicating that
1018 environmental predictors captured key bottom-up controls. However, our model did not account
1019 for top-down factors such as predation, which may also play a significant role in shaping
1020 biomass distributions, particularly in an estuary with a densely populated watershed and
1021 substantial fishing pressure.

1022 **Conclusion**

1023 This study quantifies estuarine-scale benthic macrofaunal biomass and associated carbon
1024 fluxes, including secondary production, respiration, and calcification, across the Chesapeake
1025 Bay. The results demonstrate that benthic macrofauna play a substantial and spatially structured
1026 role in estuarine carbon cycling, particularly in upper estuarine zones where biomass is highest.
1027 In these regions, benthic macrofauna respiration is a significant fraction of total available organic
1028 carbon inputs, up to 45%, while calcification accounts for a large portion of the observed
1029 alkalinity sink. These contributions vary across the salinity gradient, shaped by both
1030 environmental drivers and taxonomic composition.

1031 Patterns observed in this study suggest that benthic biomass and its associated carbon
1032 fluxes are influenced by gradients in salinity, oxygen, and organic matter inputs. The dominance
1033 of bivalves in low-salinity zones has particularly strong biogeochemical implications due to the
1034 role of bivalves in secondary production and calcification. Notably, NO_3^- emerged as a strong
1035 predictor of benthic biomass, not necessarily due to enhanced autotrophic production, but
1036 potentially reflecting allochthonous organic matter inputs that drive heterotrophic metabolism.
1037 The significant contributions of benthic communities to alkalinity consumption and DIC release
1038 highlight their potential to alter estuarine carbon chemistry in ways that depend on both
1039 biological composition and environmental conditions.

1040 To build on these results, future work should examine how benthic biomass and
1041 associated carbon fluxes vary over time in response to both natural variability and anthropogenic
1042 change. Predicting future responses is especially challenging due to the high-frequency
1043 variability in estuarine systems, which can obscure long-term signals. Understanding how POC
1044 inputs, particularly allochthonous sources, change seasonally and interannually will be critical, as

1045 will clarifying the extent to which NO₃⁻ serves as a proxy for those inputs. Long-term monitoring
1046 and modeling efforts that link changes in watershed nutrient loading, land use, and climate with
1047 benthic community dynamics will be essential for forecasting ecosystem responses and for
1048 developing more accurate, responsive biogeochemical models. These predictive relationships
1049 between benthic biomass and environmental conditions could also support management and
1050 restoration planning. By identifying areas where oxygen, salinity, or sediment improvements are
1051 most likely to enhance benthic productivity, the models provide a framework for prioritizing
1052 restoration efforts and assessing ecosystem responses to changing conditions.

1053

1054

1055

1056

1057

1058

1059

1060

1061

1062

1063

1064

1065

1066

1067

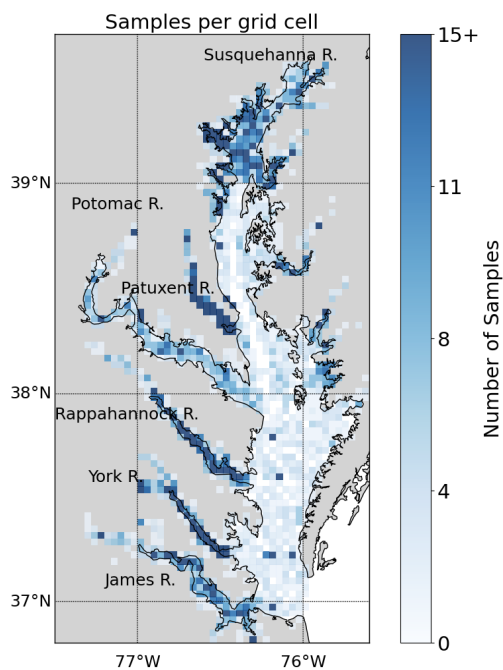
Deleted: ¶

Formatted: Font: Bold, Font color: Auto

1072 **Appendix A**

1073 ***Biomass Sampling Density***

1074 This appendix shows the spatial distribution of sampling effort for the BMP from 1995 to
1075 2022. Fig. A1 illustrates the number of samples collected in each grid cell, highlighting areas of
1076 higher and lower sampling density across the Chesapeake Bay and its tributaries.



1077
1078 Figure A1: Number of benthic samples collected in each grid cell in the summer (July 15 to
1079 September 30) from 1995 to 2022 from the Chesapeake Bay Benthic Monitoring Program. The
1080 grids are approximately square, measuring 3.5 km by 3.5 km. Each grid cell contains a time-
1081 average of each measurement collected in the cell

1082 **Appendix B**

1083 ***Carbon flux uncertainties***

1084 This appendix explains the methodology for propagating uncertainty in the benthic
 1085 macrofaunal carbon flux estimates. It outlines the parameter ranges used, the calculations for
 1086 uncertainty bounds, and the assumptions underlying these estimates. These details support the
 1087 uncertainty ranges shown in figures and tables in the Results section. Uncertainty estimates were
 1088 propagated through empirical equations using standard error propagation techniques (Taylor,
 1089 2022) assuming uncorrelated inputs and approximating relative errors when only a range of
 1090 values was available.

1091 Uncertainty for carbon-based biomass (B_c) is derived from the two different r_c values:

$$\frac{\Delta B_c}{B_c} = \frac{\Delta r_c}{r_c} \quad (B1)$$

1093 where $\Delta r_c = 0.03 \text{ g C g}^{-1}$, half the range of possible r_c values.

1094 The uncertainty for the first approach for estimating secondary production (S_1) is derived
 1095 from B_c and α :

$$\frac{\Delta S_1}{S} = \sqrt{\left(\frac{\Delta \alpha}{\alpha}\right)^2 + \left(\frac{\Delta B_c}{B_c}\right)^2} \quad (B2)$$

1097 $\Delta \alpha$ is half the range of possible α values and equals 1.695 yr^{-1} .

1098 Uncertainty in secondary production (S) arises from the multiple equations used:

$$\frac{\Delta S}{S} = \sqrt{w \left(\frac{\Delta S_1}{S_1}\right)^2 + 2w\varepsilon} \quad (B3)$$

1100 where each model is equally weighted ($w = 1/3$). Only Model 1 (Equation 5) includes an explicit
 1101 source of uncertainty, while Models 2 and 3 (Equations 7 and 8) do not. Therefore a small error
 1102 term $\varepsilon = 0.001$ was assumed for those two models.

1103 Calcification (C) uncertainty is derived from r_s and S :

Deleted: 6

Deleted: 8

Deleted: 9

$$\frac{\Delta C}{C} = \sqrt{\left(\frac{\Delta r_s}{r_s}\right)^2 + \left(\frac{\Delta S}{S}\right)^2} \quad (\text{B4})$$

where $\overline{r_s}$ has one value for *C. fluminea* and one for *P. amurensis*. $\Delta r_s = 2.5$ g CaCO₃ (g C)⁻¹ and is half the range of possible $\overline{r_s}$ values.

The uncertainty in respiration (\overline{R}) is derived solely from \overline{S} :

$$\Delta R = 2.33 \Delta S \quad (\text{B5})$$

The uncertainties in the fluxes of alkalinity and DIC ($\overline{F_{TA}}$ and $\overline{F_{DIC}}$) are also derived from \overline{C} and \overline{R} :

$$\Delta F_{TA} = \frac{-2 \Delta C}{M_{CaCO_3}} \quad (\text{B6})$$

$$\Delta F_{DIC} = \sqrt{\left(\frac{\Delta R}{M_C}\right)^2 + \left(\frac{\Delta C}{M_{CaCO_3}}\right)^2} \quad (\text{B7})$$

where M_{CaCO_3} and M_C are the molar masses of CaCO₃ and C, respectively.

Finally, we propagate the error in the flux of carbon dioxide ($\overline{F_{CO_2}}$) from the errors in $\overline{F_{TA}}$ and $\overline{F_{DIC}}$:

$$\Delta F_{CO_2} = \sqrt{\left(\frac{[CO_2] \zeta_{TA} \Delta F_{TA}}{[TA]}\right)^2 + \left(\frac{[CO_2] \zeta_{DIC} \Delta F_{DIC}}{[DIC]}\right)^2} \quad (\text{B8})$$

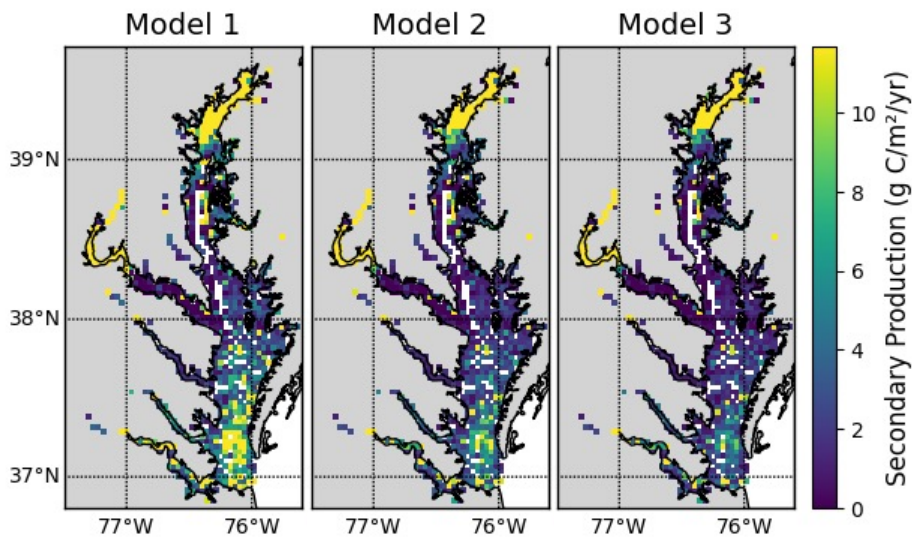
We do not consider errors in the buffer factors, [CO₂], [DIC], and [TA] in ROMS.

Appendix C

Secondary production model comparison

This appendix details the comparison of secondary production estimates from the three approaches described in Section 2.3.1. Seasonal and spatial variations are shown to illustrate the

1125 influence of temperature and other parameters on production estimates. These comparisons
1126 provide context for interpreting model differences presented in the main text.



1127
1128 Figure C1: Long-term average secondary production across the Chesapeake Bay for each of the
1129 three secondary production models.

1130 The models have similar spatial patterns (Fig. C1), which are similar to the pattern of
1131 benthic biomass (Fig. 2). Secondary production is generally higher in Model 1 than in Models 2
1132 and 3, which can be seen most clearly in the means, which are 17.92, 8.31, and 7.59 $\text{g C m}^{-2} \text{ yr}^{-1}$
1133 in Models 1, 2, and 3, respectively.

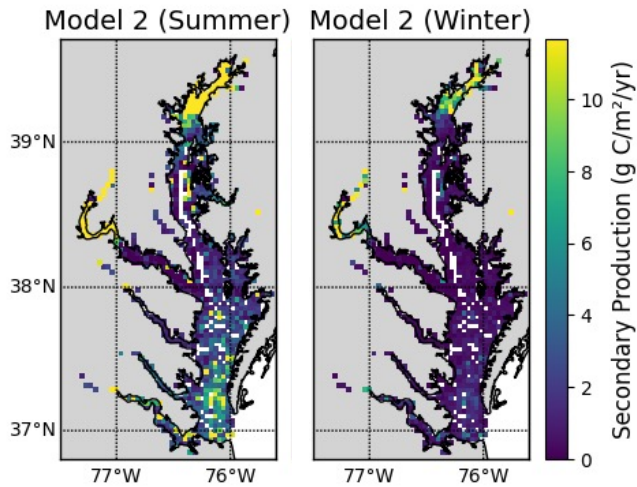


Figure C2: Seasonal sensitivity of Model 2 to bottom temperature inputs.

Fig. C2 and C3 compare secondary production between summer and winter scenarios. The summer scenario uses summer bottom water temperatures measured concurrently with biomass samples, while the winter scenario assumes a temperature of 1 °C. Fig. C2 shows the results for Model 2, which has a mean secondary production of $8.31 \text{ g C m}^{-2} \text{ yr}^{-1}$ in summer and $1.89 \text{ g C m}^{-2} \text{ yr}^{-1}$ in winter. Fig. C3 shows the results for Model 3, which has a mean secondary production of $7.59 \text{ g C m}^{-2} \text{ yr}^{-1}$ in summer and $1.44 \text{ g C m}^{-2} \text{ yr}^{-1}$ in winter. For both models, production in summer is about 5 times that of winter, as expected from the rough estimates in the Methods section. Assuming spring and fall are halfway between winter and summer, and weighting the seasons equally, the annually averaged secondary production rate would be about 60% of the summer rate.

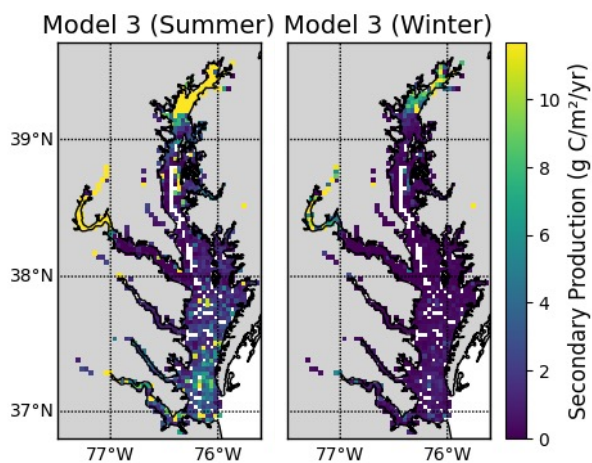
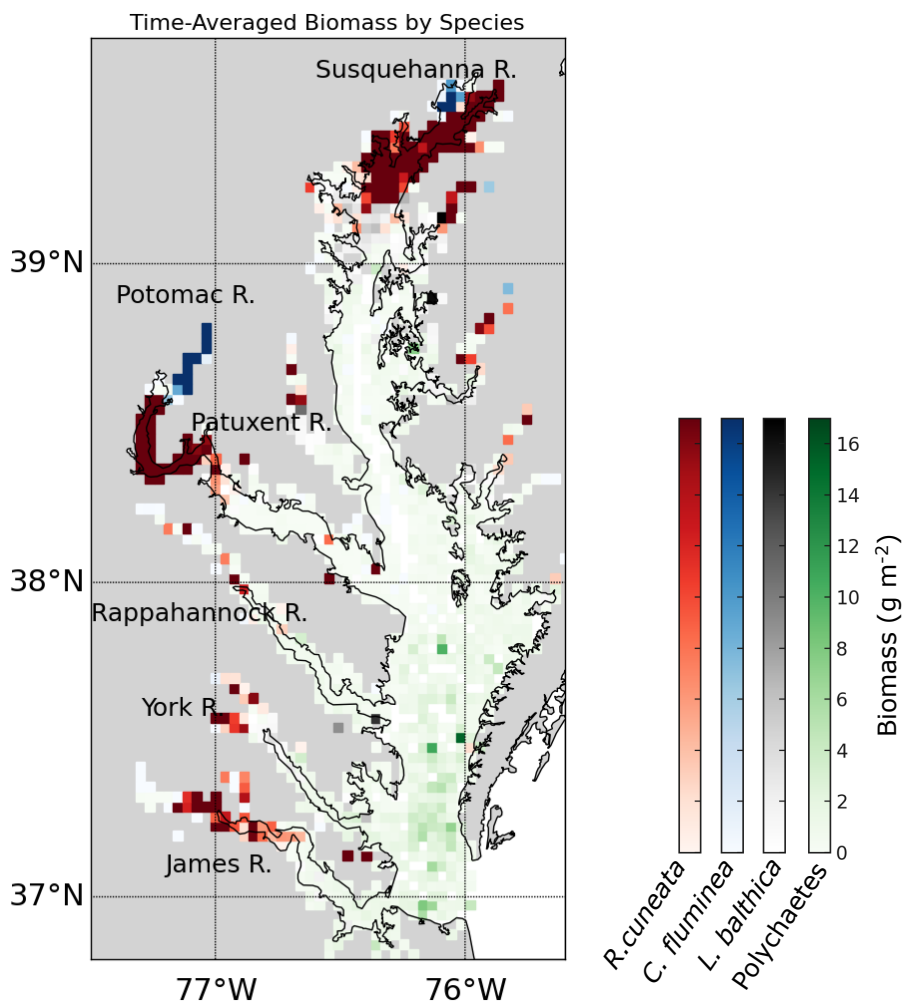


Figure C3: Seasonal sensitivity of Model 3 to bottom temperature inputs.

Appendix D

Species biomass distribution

This appendix expands on the biomass distribution results in Section 3.1 by showing detailed spatial patterns for individual species and taxonomic classes. Fig. D1 complements the summary figures in the main text, highlighting species-specific habitat associations.

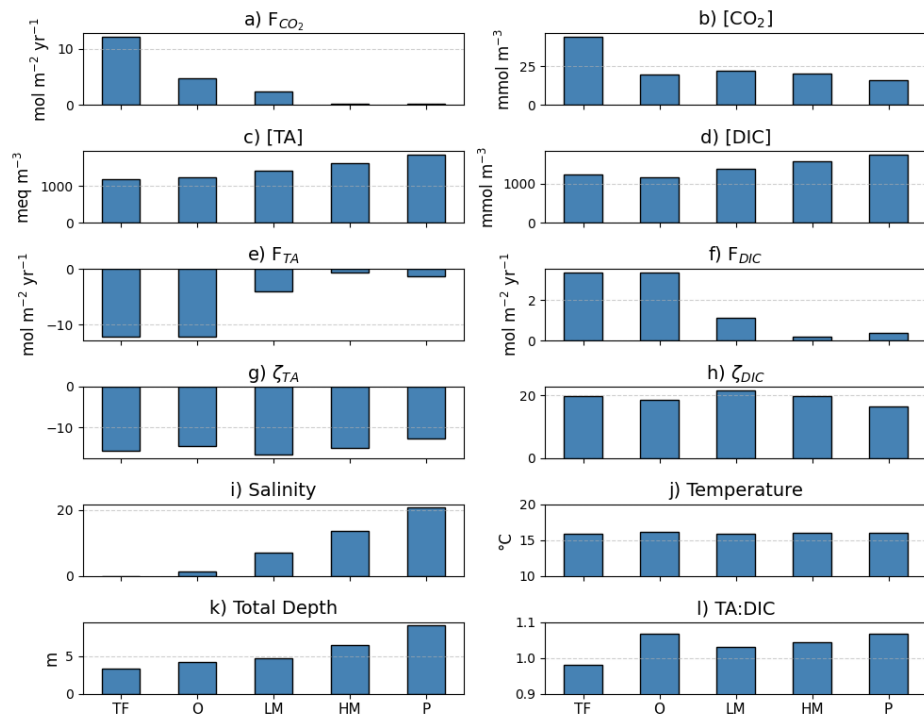


1153
 1154 Figure D1: Average summer biomass density from 1995 to 2022 from the Maryland and Virginia
 1155 Benthic Monitoring Program. Each color corresponds to a specific bivalve species (*M. balthica*,
 1156 *C. fluminea*, or *R. cuneata*) or polychaetes. The color shown on the map is the species with the
 1157 highest time-averaged biomass in that grid cell.

1158 **Appendix E**

1159 **Carbon flux-related parameters**

1160 To illustrate estuarine variability in carbonate system drivers, we summarized a suite of
1161 flux and water column properties across tidal salinity zones of the Chesapeake Bay (Fig. E1).
1162 The patterns highlight strong gradients from tidal fresh through polyhaline regions. Notably
1163 [CO₂] is elevated in tidal fresh waters, underscoring the combined influence of salinity, TA, and
1164 the TA:DIC ratio on estuarine carbonate chemistry.



1165
1166 Figure E1: Carbon flux-related parameters averaged within salinity zones of Chesapeake Bay.
1167 [CO₂] was calculated using PyCO2SYS; temperature, salinity, total depth, [TA] and [DIC] were
1168 obtained from ROMS model output. F_{TA} and F_{DIC} were calculated following Equations 12–13,
1169 ζ_{TA} and ζ_{DIC} from Equations 15–16, and F_{CO_2} from Equation 14.

Deleted: -14

Deleted: -17

Deleted: 15

1173 **Appendix F**

1174 ***GAMs evaluation***

1175 This appendix presents diagnostic plots and statistics for the generalized additive models
1176 described in Section 2.5. Residual maps, histograms, and fitted-vs-observed plots (Fig. F1) are
1177 included to evaluate model performance and identify patterns in prediction errors.

1178 A good model would have points on a modeled vs. observed scatterplot fall close to a 1:1
1179 line and have the departures from that line (residuals) be close to normally distributed. Although
1180 GAMs can handle non-normal distributions of the response variable (Guisan et al., 2002), we
1181 found the best model fit by applying a natural logarithmic transformation to the biomass. A small
1182 constant (0.0001 g m^{-2}) was added to the biomass values before applying the natural logarithmic
1183 transformation to account for zeros in the data. The resulting biomass was normally distributed
1184 after applying the natural logarithm function, so the GAM was fitted with a Gaussian distribution
1185 with an identity link function.

1186

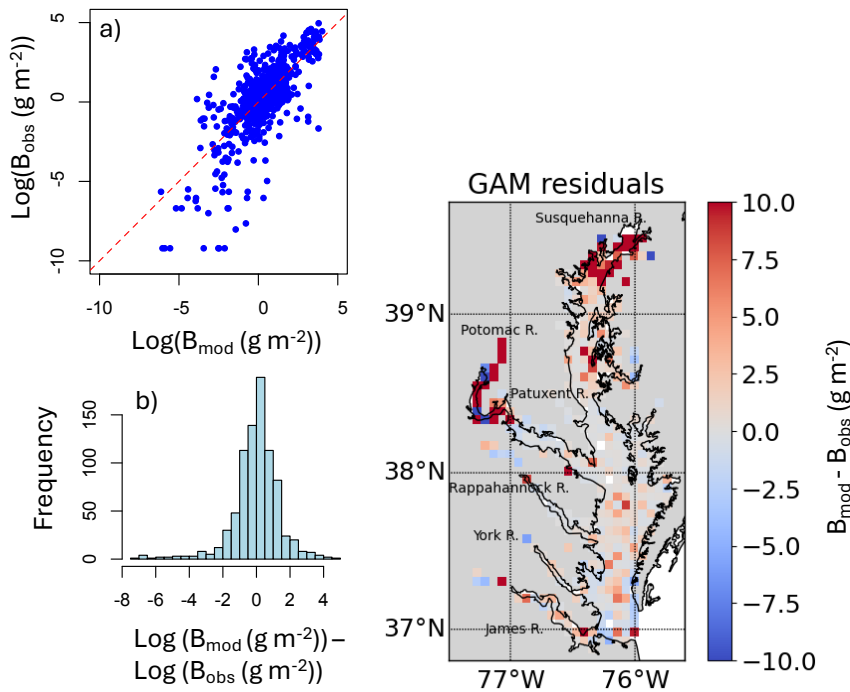


Figure F1: Evaluation of the total biomass GAM, which includes O_2 , salinity, total depth, NO_3^- , sand fraction, and water temperature as predictor variables. “Log” refers to the natural logarithm. (a) Modeled vs. observed values. (b) Histogram of biomass residuals (modeled minus observed values, $B_{\text{mod}} - B_{\text{obs}}$). (c) Spatial distribution of the residuals.

Data Availability

All data used in this study are publicly available and have been described in the Methods section. Water quality data were obtained from the *Chesapeake Bay Water Quality Monitoring Program* (<https://datahub.chesapeakebay.net/WaterQuality>), and benthic data were sourced from the *Chesapeake Bay Long-Term Benthic Monitoring Program*

1198 (<https://www.baybenthos.versar.com/data.htm>). Model output used in this study is publicly
1199 available at <https://www.seanoe.org/data/00882/99441/>.

1200

1201 **Author Contribution**

1202 SA led the research, conducted data analysis, interpreted results, and wrote the initial and
1203 subsequent drafts of the manuscript.

1204 RN conceptualized the project, defined overarching research goals, secured financial support,
1205 and contributed substantially to manuscript drafts through critical reviews, commentary, and
1206 revisions.

1207 ER provided significant insights from her expertise on the physiological responses of marine
1208 invertebrates to environmental variables, influencing the scope and direction of the study. She
1209 also substantially contributed to manuscript revisions through critical reviews and commentary.

1210 RW contributed significant expertise on benthic biomass distribution in Chesapeake Bay and
1211 generalized additive modeling techniques, shaping the analytical framework of the study. He
1212 provided critical feedback and revisions during manuscript preparation.

1213 MF provided ongoing feedback throughout the research process, particularly regarding the
1214 integration of modeling information and interpretation of results, and contributed critical
1215 commentary on multiple presentations of the work.

1216 PS consistently provided feedback and contributed modeling expertise, assisting with data
1217 interpretation and manuscript revisions through critical reviews and commentary.

1218 SD developed the original empirical models linking benthic macrofaunal biomass to carbon
1219 fluxes, laying foundational methodological contributions to the study.

1220

1221 **Competing Interests**

1222 The authors declare that they have no conflict of interest.

1223

1224 **Acknowledgements**

1225 We thank Maria Herrmann, Jill Arriola, and Alexa Labossiere for their valuable discussions and

1226 feedback that contributed to this manuscript. We also acknowledge Riley Westman and Edward

1227 Stets for providing riverine calcium input data from the USGS. Additionally, we used AI tools,

1228 including Grammarly and ChatGPT, to assist with grammar and clarity in sentence editing.

1229

1230 **Financial Support**

1231 This work is supported by the National Science Foundation (NSF) Chemical and Biological

1232 Oceanography Program under Grant Nos. OCE-2148949 (Penn State), OCE-2148950 (VIMS),

1233 and OCE-2148952 (UMCES), and by the U.S. Department of Energy's Biological and

1234 Environmental Research Program as part of the Integrated Coastal Modeling project.

1235

1236

1237

1238

1239

1240

1241

1242

1243

1244 References

- 1245 Akoglu, H. (2018). User's guide to correlation coefficients. *Turkish Journal of Emergency*
1246 *Medicine*, 18(3), 91–93. <https://doi.org/10.1016/j.tjem.2018.08.001>
- 1247 Beckwith, S. T., Byrne, R. H., & Hallock, P. (2019). Riverine calcium end-members improve
1248 coastal saturation state calculations and reveal regionally variable calcification potential.
1249 *Frontiers in Marine Science*, 6(APR). <https://doi.org/10.3389/fmars.2019.00169>
- 1250 Birchenough, S. N. R., Reiss, H., Degraer, S., Mieszkowska, N., Borja, Á., Buhl-Mortensen, L.,
1251 Braeckman, U., Craeymeersch, J., De Mesel, I., Kerckhof, F., Kröncke, I., Parra, S., Rabaut,
1252 M., Schröder, A., Van Colen, C., Van Hoey, G., Vincx, M., & Wätjen, K. (2015). Climate
1253 change and marine benthos: A review of existing research and future directions in the North
1254 Atlantic. *Wiley Interdisciplinary Reviews: Climate Change*, 6(2), 203–223.
1255 <https://doi.org/10.1002/wcc.330>
- 1256 Borja, A., Dauer, D. M., Díaz, R., Llansó, R. J., Muxika, I., Rodríguez, J. G., & Schaffner, L.
1257 (2008). Assessing estuarine benthic quality conditions in Chesapeake Bay: A comparison of
1258 three indices. *Ecological Indicators*, 8(4), 395–403.
1259 <https://doi.org/10.1016/j.ecolind.2007.05.003>
- 1260 Brey, T. (1990). Confidence limits for secondary production estimates: Application of the
1261 bootstrap to the increment summation method. *Marine Biology*, 106, 503–508.
- 1262 Brush, M. J., Mozetič, P., Francé, J., Aubry, F. B., Djakovac, T., Faganeli, J., Harris, L. A., &
1263 Niesen, M. (2020). Phytoplankton dynamics in a changing environment. In T. C. Malone,
1264 A. Malej, & J. Faganeli (Eds.), *Coastal Ecosystems in Transition: A Comparative Analysis*
1265 *of the Northern Adriatic and Chesapeake Bay* (pp. 49–74). Wiley.
1266 <https://doi.org/10.1002/9781119543626.ch4>
- 1267 Cain, T. D. (1975). Reproduction and recruitment of the brackish water clam, *Rangia cuneata* in
1268 the James River, Virginia. *Fishery Bulletin*, 73(2), 412.
1269 <https://scholarworks.wm.edu/vimsarticles/2139>
- 1270 Canuel, E. A., & Hardison, A. K. (2016). Sources, ages, and alteration of organic matter in
1271 estuaries. *Annual Review of Marine Science*, 8, 409–434. [https://doi.org/10.1146/annurev-](https://doi.org/10.1146/annurev-marine-122414-034058)
1272 [marine-122414-034058](https://doi.org/10.1146/annurev-marine-122414-034058)
- 1273 Cerco, C. F., & Noel, M. R. (2010). Monitoring, modeling, and management impacts of bivalve
1274 filter feeders in the oligohaline and tidal fresh regions of the Chesapeake Bay system.
1275 *Ecological Modelling*, 221(7), 1054–1064. <https://doi.org/10.1016/j.ecolmodel.2009.07.024>
- 1276 Chauvaud, L., Thompson, J. K., Cloern, J. E., & Thouzeau, G. (2003). Clams as CO₂ generators:
1277 The *Potamocorbula amurensis* example in San Francisco Bay. *Limnology and*
1278 *Oceanography*, 48(6), 2086–2092. <https://doi.org/10.4319/lo.2003.48.6.2086>
- 1279 Chen, C. T. A., Huang, T. H., Chen, Y. C., Bai, Y., He, X., & Kang, Y. (2013). Air–sea
1280 exchanges of CO₂ in the world's coastal seas. *Biogeosciences*, 10(10), 6509–6544.
1281 <https://doi.org/10.5194/bg-10-6509-2013>
- 1282 Chesapeake Bay Program. (n.d.). *CBP Water Quality Database (1984-present)*.
1283 *Chesapeake Bay Program analytical segmentation scheme: Revisions, decisions and rationales*,
1284 *1983–2003*. (2004).
- 1285 Dauer, D. M. (1993). Biological criteria, environmental health and estuarine macrobenthic
1286 community structure. *Marine Pollution Bulletin*, 26(5), 249–257.
1287 [https://doi.org/10.1016/0025-326X\(93\)90063-P](https://doi.org/10.1016/0025-326X(93)90063-P)

1288 Dauer, D. M., & Alden III, R. W. (1995). Long-term trends in the macrobenthos and water
 1289 quality of the lower Chesapeake Bay (1985-1991). *Marine Pollution Bulletin*, 30(12), 840–
 1290 850.

1291 Dauer, D. M., & Lane, M. F. (2010). *Quality Assurance/Quality Control Plan: Benthic*
 1292 *Biological Monitoring Program of the Lower Chesapeake Bay (July 1, 2010 to June 30,*
 1293 *2011).*

1294 Dauer, D. M., Ranasinghe, J. A., & Weisberg, S. B. (2000). Relationships between benthic
 1295 community condition, water quality, sediment quality, nutrient loads, and land use patterns
 1296 in Chesapeake Bay. *Estuaries*, 23(1), 80–96.

1297 Diaz, R. J., & Rosenberg, R. (2008). Spreading dead zones and consequences for marine
 1298 ecosystems. *Science*, 926–929. <https://www.science.org>

1299 Diaz, R. J., & Schaffner, L. C. (1990). The functional role of estuarine benthos. In M. Haire & E.
 1300 C. Krome (Eds.), *Perspectives on the Chesapeake Bay* (pp. 25–56). Chesapeake Research
 1301 Consortium.

1302 Diaz, R., & Rosenberg, R. (1995). Marine benthic hypoxia: A review of its ecological effects and
 1303 the behavioural responses of benthic macrofauna. *Oceanography and Marine Biology. An*
 1304 *Annual Review*, 33, 245–303. <https://www.researchgate.net/publication/236628341>

1305 Dolbeth, M., Cusson, M., Sousa, R., & Pardal, M. A. (2012). Secondary production as a tool for
 1306 better understanding of aquatic ecosystems. *Canadian Journal of Fisheries and Aquatic*
 1307 *Sciences*, 69(7), 1230–1253. <https://doi.org/10.1139/F2012-050>

1308 Dormann, C. F., Elith, J., Bacher, S., Buchmann, C., Carl, G., Carré, G., García Marquéz, J. R.,
 1309 Gruber, B., Lafourcade, B., Leitão, P. J., Münkemüller, T., McClean, C., Osborne, P. E.,
 1310 Reineking, B., Schröder, B., Skidmore, A. K., Zurell, D., & Lautenbach, S. (2013).
 1311 Collinearity: A review of methods to deal with it and a simulation study evaluating their
 1312 performance. *Ecography*, 36(1), 27–46.

1313 Drexler, M., & Ainsworth, C. H. (2013). Generalized additive models used to predict species
 1314 abundance in the Gulf of Mexico: An ecosystem modeling tool. *PLoS ONE*, 8(5).
 1315 <https://doi.org/10.1371/journal.pone.0064458>

1316 Edgar, G. J. (1990). The use of the size structure of benthic macrofaunal communities to estimate
 1317 faunal biomass and secondary production. *Journal of Experimental Marine Biology and*
 1318 *Ecology*, 137(3), 195–214.

1319 Egleston, E. S., Sabine, C. L., & Morel, F. M. M. (2010). Revelle revisited: Buffer factors that
 1320 quantify the response of ocean chemistry to changes in DIC and alkalinity. *Global*
 1321 *Biogeochemical Cycles*, 24(1). <https://doi.org/10.1029/2008GB003407>

1322 Ehrnsten, E., Norkko, A., Timmermann, K., & Gustafsson, B. G. (2019). Benthic-pelagic
 1323 coupling in coastal seas – Modelling macrofaunal biomass and carbon processing in
 1324 response to organic matter supply. *Journal of Marine Systems*, 196, 36–47.
 1325 <https://doi.org/10.1016/j.jmarsys.2019.04.003>

1326 Eleftheriou, A., & Moore, D. C. (2013). Macofauna techniques. *Methods for the Study of Marine*
 1327 *Benthos*, 175–251.

1328 Frankel, L. T., Friedrichs, M. A. M., St-Laurent, P., Bever, A. J., Lipcius, R. N., Bhatt, G., &
 1329 Shenk, G. W. (2022). Nitrogen reductions have decreased hypoxia in the Chesapeake Bay:
 1330 Evidence from empirical and numerical modeling. *Science of the Total Environment*, 814.
 1331 <https://doi.org/10.1016/j.scitotenv.2021.152722>

1332 Frankignoulle, M., Abril, G., Borges, A., Bourge, I., Canon, C., Delille, B., Libert, E., & Théate,
 1333 J.-M. (1998). Carbon dioxide emission from European estuaries. *Science*, 282(5388), 434–
 1334 436. <https://www.science.org>
 1335 Fulford, R. S., Breitburg, D. L., Newell, R. I. E., Kemp, W. M., & Luckenbach, M. (2007).
 1336 Effects of oyster population restoration strategies on phytoplankton biomass in Chesapeake
 1337 Bay: a flexible modeling approach. *Marine Ecology Progress Series*, 336, 43–1.
 1338 Galimany, E., Lunt, J., Freeman, C. J., Houk, J., Sauvage, T., Santos, L., Lunt, J., Kolmakova,
 1339 M., Mossop, M., Domingos, A., Philips, E. J., & Paul, V. J. (2020). Bivalve feeding
 1340 responses to microalgal bloom species in the Indian River Lagoon: the potential for top-
 1341 down control. *Estuaries and Coasts*, 43(6), 1519–1532. [https://doi.org/10.1007/s12237-020-](https://doi.org/10.1007/s12237-020-00746-9)
 1342 00746-9
 1343 Garcia, H. E., & Gordon, L. I. (1992). Oxygen solubility in seawater: Better fitting equations.
 1344 *Limnology and Oceanography*, 37(6), 1307–1312.
 1345 <https://doi.org/10.4319/lo.1992.37.6.1307>
 1346 Glud, R. N. (2008). Oxygen dynamics of marine sediments. *Marine Biology Research*, 4(4),
 1347 243–289. <https://doi.org/10.1080/17451000801888726>
 1348 Grant, J., & Thorpe, B. (1991). Effects of suspended sediment on growth, respiration, and
 1349 excretion of the soft-shell clam (*Mya arenaria*). *Canadian Journal of Fisheries and Aquatic*
 1350 *Sciences*, 48(7).
 1351 Grebmeier, J. M., Bluhm, B. A., Cooper, L. W., Denisenko, S. G., Iken, K., Kędra, M., &
 1352 Serratos, C. (2015). Time-series benthic community composition and biomass and
 1353 associated environmental characteristics in the Chukchi Sea during the RUSALCA 2004-
 1354 2012 Program. *Oceanography*, 28(3), 116–133. <https://doi.org/10.2307/24861905>
 1355 Green, M. A., Waldbusser, G. G., Reilly, S. L., Emerson, K., & O'Donnell, S. (2009). Death by
 1356 dissolution: Sediment saturation state as a mortality factor for juvenile bivalves. *Limnology*
 1357 *and Oceanography*, 54(4), 1037–1047. <https://doi.org/10.4319/lo.2009.54.4.1037>
 1358 Grüss, A., Drexler, M., & Ainsworth, C. H. (2014). Using delta generalized additive models to
 1359 produce distribution maps for spatially explicit ecosystem models. *Fisheries Research*, 159,
 1360 11–24. <https://doi.org/10.1016/j.fishres.2014.05.005>
 1361 Guisan, A., Edwards, T. C., & Hastie, T. (2002). Generalized linear and generalized additive
 1362 models in studies of species distributions: setting the scene. *Ecological Modelling*, 157(2–
 1363 3), 89. www.elsevier.com/locate/ecolmodel
 1364 Hagy, J. D. (2002). *Eutrophication, hypoxia and trophic transfer efficiency in Chesapeake Bay*
 1365 [Doctoral dissertation, University of Maryland, College Park].
 1366 <https://www.researchgate.net/publication/237005296>
 1367 Harding, L. W., Mallonee, M. E., & Perry, E. S. (2002). Toward a predictive understanding of
 1368 primary productivity in a temperate, partially stratified estuary. *Estuarine, Coastal and Shelf*
 1369 *Science*, 55(3), 437–463. <https://doi.org/10.1006/ecss.2001.0917>
 1370 Hartwell, S. I., Wright, D. A., Takacs, R., & Hocutt, C. H. (1991). Relative respiration and
 1371 feeding rates of oyster and brackish water clam in variously contaminated waters. *Marine*
 1372 *Pollution Bulletin*, 22(4), 191–197.
 1373 Hastie, T., & Tibshirani, R. (1987). Generalized additive models: Some applications. *Journal of*
 1374 *the American Statistical Association*, 82(398).
 1375 Hauke, J., & Kossowski, T. (2011). Comparison of values of Pearson's and Spearman's
 1376 correlation coefficients on the same sets of data. *Quaestiones Geographicae*, 30(2), 87–93.
 1377 <https://doi.org/10.2478/v10117-011-0021-1>

1378 Herrmann, M., Najjar, R. G., Da, F., Friedman, J. R., Friedrichs, M. A. M., Goldberger, S.,
 1379 Menendez, A., Shadwick, E. H., Stets, E. G., & St-Laurent, P. (2020). Challenges in
 1380 quantifying air-water carbon dioxide flux using estuarine water quality data: Case study for
 1381 Chesapeake Bay. *Journal of Geophysical Research: Oceans*, 125(7).
 1382 <https://doi.org/10.1029/2019JC015610>
 1383 Herrmann, M., Najjar, R. G., Kemp, W. M., Alexander, R. B., Boyer, E. W., Cai, W. J., Griffith,
 1384 P. C., Kroeger, K. D., McCallister, S. L., & Smith, R. A. (2015). Net ecosystem production
 1385 and organic carbon balance of U.S. East Coast estuaries: A synthesis approach. *Global*
 1386 *Biogeochemical Cycles*, 29(1), 96–111. <https://doi.org/10.1002/2013GB004736>
 1387 Hinson, K. E., Friedrichs, M. A. M., St-Laurent, P., Da, F., & Najjar, R. G. (2022). Extent and
 1388 causes of Chesapeake Bay warming. *Journal of the American Water Resources Association*,
 1389 58(6), 805–825. <https://doi.org/10.1111/1752-1688.12916>
 1390 Hirsch, R. M., Moyer, D. L., & Archfield, S. A. (2010). Weighted regressions on time,
 1391 discharge, and season (WRTDS), with an application to Chesapeake Bay river inputs.
 1392 *Journal of the American Water Resources Association*, 46(5), 857–880.
 1393 <https://doi.org/10.1111/j.1752-1688.2010.00482.x>
 1394 Holland, A. F., Shaughnessy, A. T., & Hiegel, M. H. (1987). Long-term variation in mesohaline
 1395 Chesapeake Bay macrobenthos: Spatial and temporal patterns. *Estuaries*, 10(3), 227–245.
 1396 Hopkins, S. H., Anderson, J. W., & Horvath, K. (1973). *The brackish water clam Rangia*
 1397 *cuneata as an indicator of ecological effects of salinity changes in coastal waters*.
 1398 Hopkinson, C. S., & Smith, E. M. (2004). Estuarine respiration: An overview of benthic, pelagic,
 1399 and whole system respiration. *Respiration in Aquatic Ecosystems*, 122–146.
 1400 Humphreys, M. P., Lewis, E. R., Sharp, J. D., & Pierrot, D. (2022). PyCO2SYS v1.8: Marine
 1401 carbonate system calculations in Python. *Geoscientific Model Development*, 15(1), 15–43.
 1402 <https://doi.org/10.5194/gmd-15-15-2022>
 1403 Irby, I. D., Friedrichs, M. A. M., Da, F., & Hinson, K. E. (2018). The competing impacts of
 1404 climate change and nutrient reductions on dissolved oxygen in Chesapeake Bay.
 1405 *Biogeosciences*, 15(9), 2649–2668. <https://doi.org/10.5194/bg-15-2649-2018>
 1406 Jakubowska, M., & Normant-Saremba, M. (2015). The effect of CO₂-induced seawater
 1407 acidification on the behaviour and metabolic rate of the Baltic clam *Macoma balthica*.
 1408 *Annales Zoologici Fennici*, 52(5–6), 353–367. <https://doi.org/10.5735/086.052.0509>
 1409 Jansson, A., Norkko, J., Dupont, S., & Norkko, A. (2015). Growth and survival in a changing
 1410 environment: Combined effects of moderate hypoxia and low pH on juvenile bivalve
 1411 *Macoma balthica*. *Journal of Sea Research*, 102, 41–47.
 1412 <https://doi.org/10.1016/j.seares.2015.04.006>
 1413 Jansson, A., Norkko, J., & Norkko, A. (2013). Effects of reduced pH on *Macoma balthica* larvae
 1414 from a system with naturally fluctuating pH-dynamics. *PLoS One*, 8(6).
 1415 <https://doi.org/10.1371/journal.pone.0068198>
 1416 Kemp, W. M., Boynton, W. R., Adolf, J. E., Boesch, D. F., Boicourt, W. C., Brush, G.,
 1417 Cornwell, J. C., Fisher, T. R., Glibert, P. M., Hagy, J. D., Harding, L. W., Houde, E. D.,
 1418 Kimmel, D. G., Miller, W. D., Newell, R. I. E., Roman, M. R., Smith, E. M., & Stevenson,
 1419 J. C. (2005). Eutrophication of Chesapeake Bay: Historical trends and ecological
 1420 interactions. *Marine Ecology Progress Series*, 303, 1–29. www.int-res.com
 1421 Kemp, W. M., Smith, E. M., Marvin-DiPasquale, M., & Boynton, W. R. (1997). Organic carbon
 1422 balance and net ecosystem metabolism in Chesapeake Bay. *Marine Ecology Progress*
 1423 *Series*, 150, 229–248.

1424 Kroeker, K. J., Kordas, R. L., Crim, R., Hendriks, I. E., Ramajo, L., Singh, G. S., Duarte, C. M.,
1425 & Gattuso, J. P. (2013). Impacts of ocean acidification on marine organisms: quantifying
1426 sensitivities and interaction with warming. *Global Change Biology*, 19(6), 1884–1896.
1427 <https://doi.org/10.1111/gcb.12179>

1428 Levin, L. A., Ekau, W., Gooday, A. J., Jorissen, F., Middelburg, J. J., Naqvi, S. W. A., Neira, C.,
1429 Rabalais, N. N., & Zhang, J. (2009). Effects of natural and human-induced hypoxia on
1430 coastal benthos. In *Biogeosciences* (Vol. 6). www.biogeosciences.net/6/2063/2009/

1431 Little, S., Wood, P. J., & Elliott, M. (2017). Quantifying salinity-induced changes on estuarine
1432 benthic fauna: The potential implications of climate change. *Estuarine, Coastal and Shelf
1433 Science*, 198, 610–625. <https://doi.org/10.1016/j.ecss.2016.07.020>

1434 Llansó, R. J. (2002). *Methods for calculating the Chesapeake Bay benthic index of biotic
1435 integrity*. <http://www.baybenthos.versar.com>

1436 Llansó, R. J., & Scott, L. (2011). *Chesapeake Bay water quality monitoring program: Long-term
1437 benthic monitoring and assessment component, quality assurance project plan, 2011–2012*.

1438 Llansó, R. J., & Zaveta, D. (2017). *Chesapeake Bay water quality monitoring program: Long-
1439 term benthic monitoring and assessment component level 1 comprehensive report, July
1440 1984 – December 2016 (Volume 1)*.

1441 Marsh, A. G., & Tenore, K. R. (1990). The role of nutrition in regulating the population
1442 dynamics of opportunistic, surface deposit feeders in a mesohaline community. *Limnology
1443 and Oceanography*, 35(3), 710–724. <https://doi.org/10.4319/lo.1990.35.3.0710>

1444 Meysman, F. J. R., tax, J. J., & Heip, C. H. R. (2006). Bioturbation: A fresh look at Darwin's last
1445 idea. *Trends in Ecology and Evolution*, 21(12), 688–695.
1446 <https://doi.org/10.1016/j.tree.2006.08.002>

1447 Middelburg, J. J. (2018). Reviews and syntheses: To the bottom of carbon processing at the
1448 seafloor. In *Biogeosciences* (Vol. 15, Issue 2, pp. 413–427). Copernicus GmbH.
1449 <https://doi.org/10.5194/bg-15-413-2018>

1450 Middelburg, J. J., Soetaert, K., & Hagens, M. (2020). Ocean alkalinity, buffering and
1451 biogeochemical processes. *Reviews of Geophysics*, 58(3).
1452 <https://doi.org/10.1029/2019RG000681>

1453 Mo, C., & Neilson, B. (1994). Standardization of oyster soft tissue dry weight measurements.
1454 *Water Research*, 28(1), 243–246.

1455 Murphy, R. R., Kemp, W. M., & Ball, W. P. (2011). Long-term trends in Chesapeake Bay
1456 seasonal hypoxia, stratification, and nutrient loading. *Estuaries and Coasts*, 34(6), 1293–
1457 1309. <https://doi.org/10.1007/s12237-011-9413-7>

1458 Murphy, R. R., Perlman, E., Ball, W. P., & Curriero, F. C. (2015). Water-distance-based kriging
1459 in Chesapeake Bay. *Journal of Hydrologic Engineering*, 20(9).
1460 [https://doi.org/10.1061/\(asce\)he.1943-5584.0001135](https://doi.org/10.1061/(asce)he.1943-5584.0001135)

1461 Najjar, R. G., Herrmann, M., Alexander, R., Boyer, E. W., Burdige, D. J., Butman, D., Cai, W.
1462 J., Canuel, E. A., Chen, R. F., Friedrichs, M. A. M., Feagin, R. A., Griffith, P. C., Hinson,
1463 A. L., Holmquist, J. R., Hu, X., Kemp, W. M., Kroeger, K. D., Mannino, A., McCallister, S.
1464 L., ... Zimmerman, R. C. (2018). Carbon budget of tidal wetlands, estuaries, and shelf
1465 waters of Eastern North America. *Global Biogeochemical Cycles*, 32(3), 389–416.
1466 <https://doi.org/10.1002/2017GB005790>

1467 Najjar, R. G., Herrmann, M., Cintrón Del Valle, S. M., Friedman, J. R., Friedrichs, M. A. M.,
1468 Harris, L. A., Shadwick, E. H., Stets, E. G., & Woodland, R. J. (2020). Alkalinity in tidal

tributaries of the Chesapeake Bay. *Journal of Geophysical Research: Oceans*, 125(1).
<https://doi.org/10.1029/2019JC015597>

Nakamura, Y., & Kerciku, F. (2000). Effects of filter-feeding bivalves on the distribution of water quality and nutrient cycling in a eutrophic coastal lagoon. *Journal of Marine Systems*, 26, 209–221. www.elsevier.nl/locate/jmarsys

Newell, R. I. E. (1988). Ecological changes in Chesapeake Bay: are they the result of overharvesting the American oyster, *Crassostrea virginica*. *Understanding the Estuary: Advances in Chesapeake Bay Research*, 129, 536–546.

Newell, R. I. E., & Ott, J. A. (2011). Macrobenthic communities and eutrophication. *Ecosystems at the Land-Sea Margin: Drainage Basin to Coastal Sea*, 55, 265–293.
<https://doi.org/10.1029/ce055p0265>

Ni, W., Li, M., Ross, A. C., & Najjar, R. G. (2019). Large projected decline in dissolved oxygen in a eutrophic estuary due to climate change. *Journal of Geophysical Research: Oceans*, 124(11), 8271–8289. <https://doi.org/10.1029/2019JC015274>

Olson, M. (2012). *Guide to using Chesapeake Bay Program water quality monitoring data*.

Pearson, T. H., & Rosenberg, R. (1978). Macrobenthic succession in relation to organic enrichment and pollution of the marine environment. *Oceanography and Marine Biology: An Annual Review*, 16, 229–311.

Phelps H.L. (1994). The Asiatic clam (*Corbicula fluminea*) invasion and system-level ecological change in the Potomac River estuary near Washington, DC. *Estuaries*, 17(3), 614–621.

Redfield, A. C. (1963). The influence of organisms on the composition of seawater. *The Sea*, 26–77.

Rodil, I. F., Lohrer, A. M., Attard, K. M., Thrush, S. F., & Norkko, A. (2022). Positive contribution of macrofaunal biodiversity to secondary production and seagrass carbon metabolism. *Ecology*, 103(4). <https://doi.org/10.1002/ecy.3648>

Rosenberg, R. (1995). Benthic marine fauna structured by hydrodynamic processes and food availability. *Netherlands Journal of Sea Research*, 34(4), 303–317.

Rousi, H., Korpinen, S., & Bonsdorff, E. (2019). Brackish-water benthic fauna under fluctuating environmental conditions: the role of eutrophication, hypoxia, and global change. *Frontiers in Marine Science*, 6(JUL), 464. <https://doi.org/10.3389/fmars.2019.00464>

Schratzberger, M., & Ingels, J. (2018). Meiofauna matters: the roles of meiofauna in benthic ecosystems. *Journal of Experimental Marine Biology and Ecology*, 502, 12–25.
<https://doi.org/10.1016/j.jembe.2017.01.007>

Schwinghamer, P., Hargrave, B., Peer, D., & Hawkins, C. M. (1986). Partitioning of production and respiration among size groups of organisms in an intertidal benthic community. *Marine Ecology Progress Series*, 31(2), 131–142.

Seitz, R. D., Dauer, D. M., Llansó, R. J., & Long, W. C. (2009). Broad-scale effects of hypoxia on benthic community structure in Chesapeake Bay, USA. *Journal of Experimental Marine Biology and Ecology*, 381(SUPPL.), <https://doi.org/10.1016/j.jembe.2009.07.004>

Seitz, R., Lipcius, R. N., Olmstead, N. H., Seebo, M. S., & Lambert, D. M. (2006). Influence of shallow-water habitats and shoreline development on abundance, biomass, and diversity of benthic prey and predators in Chesapeake Bay. *Marine Ecology Progress Series*, 326, 11–27.

Shchepetkin, A. F., & McWilliams, J. C. (2005). The regional oceanic modeling system (ROMS): A split-explicit, free-surface, topography-following-coordinate oceanic model. *Ocean Modelling*, 9(4), 347–404. <https://doi.org/10.1016/j.ocemod.2004.08.002>

1515 Simon N. Wood. (2017). *Generalized Additive Models* (2nd ed.).

1516 Smith, M., Paperno, R., Flaherty-Walia, K., & Markwith, S. (2023). Species Distributions in a

1517 Changing Estuary: Predictions Under Future Climate Change, Sea-Level Rise, and

1518 Watershed Restoration. *Estuaries and Coasts*, 46(6). [https://doi.org/10.1007/s12237-023-](https://doi.org/10.1007/s12237-023-01219-5)

1519 01219-5

1520 Snelgrove, P. V. R. (1997). The importance of marine sediment biodiversity in ecosystem

1521 processes. *Ambio*, 26(8), 578–583. <https://doi.org/https://www.jstor.org/stable/4314672>

1522 Snelgrove, P. V. R. (1999). Snelgrove, P. V. (1999). Getting to the bottom of marine

1523 biodiversity: sedimentary habitats: ocean bottoms are the most widespread habitat on earth

1524 and support high biodiversity and key ecosystem services. *BioScience*, 42(2), 129–138.

1525 www.jstor.org

1526 Snelgrove, P. V. R., Soetaert, K., Solan, M., Thrush, S., Wei, C. L., Danovaro, R., Fulweiler, R.

1527 W., Kitazato, H., Ingole, B., Norkko, A., Parkes, R. J., & Volkenborn, N. (2018). Global

1528 carbon cycling on a heterogeneous seafloor. *Trends in Ecology & Evolution*, 33(2), 96–105.

1529 <https://doi.org/10.1016/j.tree.2017.11.004>

1530 Sousa, R., Antunes, C., & Guilhermino, L. (2008). Ecology of the invasive Asian clam *Corbicula*

1531 *fluminea* (Müller, 1774) in aquatic ecosystems: An overview. In *Annales de Limnologie-*

1532 *International Journal of Limnology* (Vol. 44, Issue 2, pp. 85–94).

1533 <https://doi.org/10.1051/limn:2008017>

1534 St-Laurent, P., & Friedrichs, M. A. M. (2024a). An atlas for physical and biogeochemical

1535 conditions in the Chesapeake Bay. *SEANO*.

1536 St-Laurent, P., & Friedrichs, M. A. M. (2024b). On the sensitivity of coastal hypoxia to its

1537 external physical forcings. *Journal of Advances in Modeling Earth Systems*, 16(1).

1538 <https://doi.org/10.1029/2023MS003845>

1539 Sturdivant, S. K., Seitz, R. D., & Diaz, R. J. (2013). Effects of seasonal hypoxia on macrobenthic

1540 production and function in the Rappahannock River, Virginia, USA. *Marine Ecology*

1541 *Progress Series*, 490, 53–68. <https://doi.org/10.3354/meps10470>

1542 Symonds, M. R. E., & Moussalli, A. (2011). A brief guide to model selection, multimodel

1543 inference and model averaging in behavioural ecology using Akaike's information criterion.

1544 *Behavioral Ecology and Sociobiology*, 65(1), 13–21. [https://doi.org/10.1007/s00265-010-](https://doi.org/10.1007/s00265-010-1037-6)

1545 1037-6

1546 Taylor, J. R. (2022). *An introduction to error analysis: the study of uncertainties in physical*

1547 *measurements*. MIT Press.

1548 Testa, J. M., Faganeli, J., Giani, M., Brush, M. J., De Vittor, C., Boynton, W. R., Covelli, S.,

1549 Woodland, R. J., Kovač, N., & Michael Kemp, W. (2020a). Advances in our understanding

1550 of pelagic-benthic coupling. In T. C. Malone, A. Malej, & J. Faganeli (Eds.), *Coastal*

1551 *Ecosystems in Transition: A Comparative Analysis of the Northern Adriatic and*

1552 *Chesapeake Bay* (pp. 147–175). Wiley. <https://doi.org/10.1002/9781119543626.ch8>

1553 Testa, J. M., Faganeli, J., Giani, M., Brush, M. J., De Vittor, C., Boynton, W. R., Covelli, S.,

1554 Woodland, R. J., Kovač, N., & Michael Kemp, W. (2020b). Advances in our understanding

1555 of Pelagic-Benthic Coupling. In T. C. Malone, A. Malej, & J. Faganeli (Eds.), *Coastal*

1556 *Ecosystems in Transition: A Comparative Analysis of the Northern Adriatic and*

1557 *Chesapeake Bay* (pp. 147–175). Wiley. <https://doi.org/10.1002/9781119543626.ch8>

1558 Thomsen, J., Haynert, K., Wegner, K. M., & Melzner, F. (2015). Impact of seawater carbonate

1559 chemistry on the calcification of marine bivalves. *Biogeosciences*, 12(14), 4209–4220.

1560 <https://doi.org/10.5194/bg-12-4209-2015>

1561 Tumbiolo, M. L., & Downing, J. A. (1994). An empirical model for the prediction of secondary
 1562 production in marine benthic invertebrate populations. *Marine Ecology Progress Series*,
 1563 114(1), 165–174.
 1564 Tuszer-Kunc, J., Normant-Saremba, M., & Rychter, A. (2020). The combination of low salinity
 1565 and low temperature can limit the colonisation success of the non-native bivalve *Rangia*
 1566 *cuneata* in brackish Baltic waters. *Journal of Experimental Marine Biology and Ecology*,
 1567 524. <https://doi.org/10.1016/j.jembe.2019.151228>
 1568 Vaquer-Sunyer, R., & Duarte, C. M. (2008). Thresholds of hypoxia for marine biodiversity.
 1569 *Proceeds of the National Academy of Sciences*, 105(40), 15452–15457.
 1570 www.pnas.org/cgi/content/full/
 1571 Waldbusser, G. G., Hales, B., Langdon, C. J., Haley, B. A., Schrader, P., Brunner, E. L., Gray,
 1572 M. W., Miller, C. A., & Gimenez, I. (2015). Saturation-state sensitivity of marine bivalve
 1573 larvae to ocean acidification. *Nature Climate Change*, 5(3), 273–280.
 1574 <https://doi.org/10.1038/nclimate2479>
 1575 Waldbusser, G. G., Powell, E. N., & Mann, R. (2013). Ecosystem effects of shell aggregations
 1576 and cycling in coastal waters: an example of Chesapeake Bay oyster reefs. *Ecology*, 94(4),
 1577 895–903. <https://doi.org/10.1890/12-1179.1>
 1578 Ware, J. R., Smith, S. V., & Reaka-Kudla, M. L. (1992). Coral reefs: Sources or sinks of
 1579 atmospheric CO₂? *Coral Reefs*, 11(3), 127–130.
 1580 Weisberg, S., Ranasinghe, A., Schaffner Robert J Diaz, L. C., Dauer, D. M., & Frithsen, F. B.
 1581 (1997). An estuarine benthic index of biotic integrity (B-IBI) for Chesapeake Bay.
 1582 *Estuaries*, 20(1), 149–158.
 1583 Wilson, J. G., & Fleeger, J. W. (2023). Estuarine benthos. In B. C. Crump, J. M. Testa, & K. H.
 1584 Dunton (Eds.), *Estuarine Ecology* (3rd ed., pp. 253–273). Wiley.
 1585 Wolf-Gladrow, D. A., Zeebe, R. E., Klaas, C., Körtzinger, A., & Dickson, A. G. (2007). Total
 1586 alkalinity: The explicit conservative expression and its application to biogeochemical
 1587 processes. *Marine Chemistry*, 106(1-2 SPEC. ISS.), 287–300.
 1588 <https://doi.org/10.1016/j.marchem.2007.01.006>
 1589 Wood, S. N. (2011). Fast stable restricted maximum likelihood and marginal likelihood
 1590 estimation of semiparametric generalized linear models. *Journal of the Royal Statistical*
 1591 *Society Series B: Statistical Methodology*, 73(1), 3–36.
 1592 <https://academic.oup.com/jrsssb/article/73/1/3/7034726>
 1593 Woodland, R. J., Buchheister, A., Latour, R. J., Lozano, C., Houde, E., Sweetman, C. J.,
 1594 Fabrizio, M. C., & Tuckey, T. D. (2021). Environmental drivers of forage fishes and benthic
 1595 invertebrates at multiple spatial scales in a large temperate estuary. *Estuaries and Coasts*,
 1596 44(4), 921–938. <https://doi.org/10.1007/s12237-020-00835-9>
 1597 Woodland, R. J., & Testa, J. M. (2020). Response of benthic biodiversity to climate-sensitive
 1598 regional and local conditions in a complex estuarine system. In V. Lyubchich, Y. R. Gel, K.
 1599 H. Kilbourne, T. J. Miller, N. K. Newlands, & A. B. Smith (Eds.), *Evaluating Climate*
 1600 *Change IMpacts* (Vol. 1, pp. 87–22). CRC Press.
 1601 Zhang, Q., & Blomquist, J. D. (2018). Watershed export of fine sediment, organic carbon, and
 1602 chlorophyll-a to Chesapeake Bay: Spatial and temporal patterns in 1984–2016. *Science of*
 1603 *the Total Environment*, 619–620, 1066–1078.
 1604 <https://doi.org/10.1016/j.scitotenv.2017.10.279>
 1605 Zhang, Q., Fisher, T. R., Trentacoste, E. M., Buchanan, C., Gustafson, A. B., Karrh, R., Murphy,
 1606 R. R., Keisman, J., Wu, C., Tian, R., Testa, J. M., & Tango, P. J. (2021). Nutrient limitation

1607 of phytoplankton in Chesapeake Bay: Development of an empirical approach for water-
1608 quality management. *Water Research*, 188. <https://doi.org/10.1016/j.watres.2020.116407>
1609 Zheng, G., & DiGiacomo, P. M. (2020). Linkages between phytoplankton and bottom oxygen in
1610 the Chesapeake Bay. *Journal of Geophysical Research: Oceans*, 125(2).
1611 <https://doi.org/10.1029/2019JC015650>
1612

1613

Page 5: [1] Deleted	Ajayi, Seyi	11/7/25 12:26:00 PM
---------------------	-------------	---------------------



Page 5: [2] Deleted	Ajayi, Seyi	11/7/25 12:26:00 PM
---------------------	-------------	---------------------



Page 5: [3] Deleted	Ajayi, Seyi	11/7/25 12:26:00 PM
---------------------	-------------	---------------------

